THE FASEB JOURNAL • RESEARCH • www.fasebj.org

Developmental abnormalities in cortical GABAergic system in mice lacking mGlu3 metabotropic glutamate receptors

Tiziana Imbriglio,[*,1] Remy Verhaeghe,[*,1] Katiuscia Martinello,[†] Maria Teresa Pascarelli,[*,††] Giuseppina Chece,[*] Domenico Bucci,[†] Serena Notartomaso,[†] Miriana Quattromani,[‡] Giada Mascio,[†] Francesco Scalabrì,[§] Antonio Simeone,[¶] Stefania Maccari,[‖,#] Claudio Del Percio,[*] Tadeusz Wieloch,[‡] Sergio Fucile,[*,†] Claudio Babiloni,[*,] Giuseppe Battaglia,[*,†] Cristina Limatola,[*,†] Ferdinando Nicoletti,[*,†,2] and Milena Cannella[†]**

[*]Department of Physiology and Pharmacology "V. Erspamer," and [#]Department of Science and Medical - Surgical Biotechnology, University Sapienza of Rome, Italy; [†]Istituto di Ricovero e Cura a Carattere Scientifico (IRCCS) Neuromed, Pozzilli (IS), Italy; [††]Oasi Research Institute – Istituto di Ricovero e Cura a Carattere Scientifico (IRCCS), Troina (EN), Italy; [‡]Laboratory for Experimental Brain Research, Department of Clinical Sciences, Lund University, Sweden; [§]Istituto di Ricerca Biologia Molecolare (IRBM) Science Park S.p.A., Pomezia, Rome, Italy; [¶]Institute of Genetics and Biophysics "Adriano Buzzati-Traverso", Centro Nazionale Ricerche (CNR), Naples, Italy; [‖]University of Lille, Centre National de la Recherche Scientifique (CNRS), Unité Mixte de Recherche (UMR) 8576, UGSF, Unité de Glycobiologie Structurale et Fonctionnelle, Lille, France; and **Hospital San Raffaele Cassino, Cassino (FR), Italy

ABSTRACT: Polymorphic variants of the gene encoding for metabotropic glutamate receptor 3 (mGlu3) are linked to schizophrenia. Because abnormalities of cortical GABAergic interneurons lie at the core of the pathophysiology of schizophrenia, we examined whether mGlu3 receptors influence the developmental trajectory of cortical GABAergic transmission in the postnatal life. mGlu3$^{-/-}$ mice showed robust changes in the expression of interneuron-related genes in the prefrontal cortex (PFC), including large reductions in the expression of parvalbumin (PV) and the GluN1 subunit of NMDA receptors. The number of cortical cells enwrapped by perineuronal nets was increased in mGlu3$^{-/-}$ mice, suggesting that mGlu3 receptors shape the temporal window of plasticity of PV^{+} interneurons. Electrophysiological measurements of $GABA_A$ receptor–mediated responses revealed a more depolarized reversal potential of GABA currents in the somata of PFC pyramidal neurons in mGlu3$^{-/-}$ mice at postnatal d 9 associated with a reduced expression of the K^+/Cl^- symporter. Finally, adult mGlu3$^{-/-}$ mice showed lower power in electroencephalographic rhythms at 1–45 Hz in quiet wakefulness as compared with their wild-type counterparts. These findings suggest that mGlu3 receptors have a strong impact on the development of cortical GABAergic transmission and cortical neural synchronization mechanisms corroborating the concept that genetic variants of mGlu3 receptors may predispose to psychiatric disorders.—Imbriglio, T., Verhaeghe, R., Martinello, K., Pascarelli, M. T., Chece, G., Bucci, D., Notartomaso, S., Quattromani, M., Mascio, G., Scalabrì, F., Simeone, A., Maccari, S., Del Percio, C., Wieloch, T., Fucile, S., Babiloni, C., Battaglia, G., Limatola, C., Nicoletti, F., Cannella, M. Developmental abnormalities in cortical GABAergic system in mice lacking mGlu3 metabotropic glutamate receptors. FASEB J. 33, 000–000 (2019). www.fasebj.org

KEY WORDS: mGlu3 receptors · cortical interneurons · development · oscillations · perineuronal nets

Metabotropic glutamate (mGlu) receptors are linked to the pathophysiology of schizophrenia and are candidate drug targets for therapeutic intervention (1, 2). mGlu receptors form a family of 8 subtypes, of which mGlu1 and mGlu5 receptors are coupled to $G_{q/11}$, whereas all other subtypes are coupled to $G_{i/o}$ (3). Selective disruption of mGlu5

ABBREVIATIONS: ACSF, artificial cerebrospinal fluid; Arx, aristaless; bHLH, basic helix-loop-helix; CB1, cannabinoid receptor type 1; CCK, cholecystokinine; CSPG, chondroitin sulfate proteoglycan; EEG, electroencephalographic; E_{GABA}, reversal potential of GABA currents; GAD, glutamate decarboxylase; GRM3, mGlu3 receptor gene; KCC2, K^+/Cl^- symporter; LSD, least significant difference; mGlu, metabotropic glutamate; MP, membrane potential; NPY, neuropeptide Y; PAM, positive allosteric modulator; PFC, prefrontal cortex; PND, postnatal day; PNN, perineuronal net; PV, parvalbumin; RTN, reticular thalamic nucleus; Sst, somatostatin; VIP, vasoactive intestinal peptide; WFA, *Wisteria floribunda* agglutinin

[1] These authors contributed equally to this work.

[2] Correspondence: Istituto di Ricovero e Cura a Carattere Scientifico (IRCCS) Neuromed, Pozzilli (IS), Italy. E-mail: ferdinandonicoletti@hotmail.com

doi: 10.1096/fj.201901093RRR
This article includes supplemental data. Please visit *http://www.fasebj.org* to obtain this information.

receptors in parvalbumin $(PV)^+$ GABAergic interneurons in mice induces neurophysiological and behavioral abnormalities that are reminiscent of those occurring in schizophrenia (4), and positive allosteric modulators (PAMs) of mGlu5 receptors are under development as antipsychotic agents (5).

Drugs that activate both mGlu2 and mGlu3 receptors have shown efficacy in behavioral tests that are predictive of antipsychotic activity (6), and pomaglumetad, a prodrug of the mGlu2/3 receptor agonist, LY404039, showed therapeutic efficacy in subgroups of patients affected by schizophrenia (7). The antipsychotic activity of mGlu2/3 receptor agonists appears to be mediated by mGlu2 receptors because it is abolished in mGlu2 receptor knockout mice and is shared by mGlu2 receptor PAMs (8, 9). However, the mGlu2-centric hypothesis of schizophrenia is challenged by the following observations: *1*) mGlu3 receptor knockout mice show behavioral and neurochemical abnormalities that are consistent with a psychotic-like phenotype (10, 11); *2*) alterations in mGlu3 receptor dimerization have been found in the frontal cortex of patients with schizophrenia (12); and *3*) polymorphic variants of the mGlu3 receptor gene (GRM3) are associated with schizophrenia (13, 14). A relation between mGlu3 receptors and schizophrenia is strenghtened by the finding that activation of mGlu3 receptors boosts mGlu5 receptor signaling, and mGlu3 and mGlu5 receptors interact in the induction of long-term depression in the prefrontal cortex (PFC) (15). Expression of mGlu3 receptors is widespread in the CNS. *In situ* hybridization and immunohistochemical analysis showed high levels of expression in the reticular thalamic nucleus (RTN) and moderate levels of expression in the cerebral cortex, amygdala, and other brain regions (16–18). mGlu3 receptors are present in both neurons and glial cells, and they are expressed in all components of the tripartite synapse (*i.e.*, axon terminals, dendritic spines, and surrounding astrocytes) (18). mGlu3 and mGlu5 receptors share the same developmental pattern of expression. The transcript of both receptor subtypes is highly expressed in the cerebral cortex and other brain regions in the first 7–9 d of postnatal development, and expression declines afterward. This pattern is not shared by other mGlu receptor subtypes (19).

The first 9 d of postnatal life are critical for terminal differentiation and functional specialization of cortical PV^+ GABAergic interneurons, which innervate axon segment of pyramidal neurons, and play a key role in network oscillations (20). In addition, profound changes in GABAergic transmission occur during early postnatal life, such as the excitatory-to-inhibitory GABA shift because of a sharp reduction in intracellular Cl^- concentrations (21).

Starting after the second week of postnatal life, cortical PV^+ interneurons in mice begin to be enwrapped by highly organized, lattice-like macromolecular structures of the extracellular matrix called perineuronal nets (PNNs), which are formed by a linear nonsulfated hyaluronic acid polymer joined to chondroitin sulfate proteoglycans (CSPGs) through a series of linking proteins (22–25). It has been proposed that PNNs restrain the plasticity of PV^+ interneurons, and their deposition concides with the closure of critical periods of CNS plasticity (26). In the PFC, PNNs have been shown to regulate the inhibitory currents onto pyramidal neurons, thereby influencing cortical network activity and mechanisms of neuronal plasticity (27, 28). Thus, an optimal level of PNNs within the appropriate time windows may be essential for the correct balance between excitation and inhibition underlying cognitive function.

Preclinical studies and analysis of human brain tissue suggest that abnormalities in PV^+ GABAergic interneurons are linked to the pathophysiology of schizophrenia (29). Reduced levels of neurochemical markers of PV^+ interneurons are found in the PFC of subjects with schizophrenia (30–34). PV^+ interneurons play a key role in the generation of electroencephalographic (EEG) oscillations at γ-frequency during working memory (35), and this neurophysiological mechanism may be abnormal in schizophrenia (36, 37). Changes in the density of PNNs have also been reported in the PFC and other brain regions of individuals affected by schizophrenia (34, 38–41).

We hypothesized that mGlu3 receptors may affect not only the development and functional specialization of PV^+ GABAergic interneurons but also large-scale brain neural synchronization and desynchronization mechanisms underling cortical EEG oscillations in quiet wakefulness. This hypothesis was tested by a multidisciplinary approach based on: *1*) expression analysis of selected neurochemical markers of PV^+ and other GABAergic interneurons in the PFC across postnatal development; *2*) electrophysiological analysis of GABAergic transmission in the PFC; *3*) immunohistochemical analysis of PNNs; and *4*) evaluation of cortical EEG oscillations underpinning neural synchronization and desynchronization mechanisms in quiet wakefulness. The whole analysis was performed in wild-type and mGlu3 receptor knockout ($mGlu3^{-/-}$) mice. When appropriate, $mGlu2^{-/-}$ mice were used for comparative purposes.

MATERIALS AND METHODS

Animals

Adult male and female CD1 mice were housed under controlled conditions ($T = 22°C$; humidity = 40%) on a 12-h light/dark cycle with food and water *ad libitum*. Experiments were performed following the *Guide for the Care and Use of Laboratory Animals* (National Institutes of Health, Bethesda, MD, USA) to minimize the number of animals and animal suffering. The experimental protocol was approved by the Ethical Committee of Neuromed Institute (Pozzilli, Italy) and approved as a current research project at Istituto di Ricovero e Cura a Carattere Scientifico (IRCCS) Neuromed by the Italian Ministry of Health. mGlu2 and mGlu3 receptor knockout mice ($mGlu2^{-/-}$ and $mGlu3^{-/-}$ mice) with a CD1 genetic background were kindly provided by Eli Lilly and Co. (Indianapolis, IN, USA). Mouse strains were originally generated by homologous recombination (42). One male and 2 females of $mGlu2^{-/-}$, $mGlu3^{-/-}$, and wild-type CD1 mice were housed for homozygous mating. We did not use littermates generated by heterozygous mating to minimize the number of mice (experiments were performed exclusively on homozygous mice). For appropriate embryonic staging, noon of the day of vaginal plug detection was designated as embryonic day (E)0.5. E12.5 embryos were used for immunohistochemical analysis of homobox and basic helix-loop-helix (bHLH) genes. Mice at

postnatal days (PNDs) 1, 9, 21, 30, and 75 were used for biochemical analysis of interneuron-related genes, for electrophysiological analysis of GABAergic neurotransmission, and for immunohistochemical analysis of PNNs. Wild-type and mGlu3$^{-/-}$ mice at 75 PNDs were used for EEG recording.

Immunohistochemical analysis of homeobox and bHLH genes

Embryos were fixed in 4% paraformaldehyde and embedded in wax. Adjacent sections were processed for immunohistochemistry. Sections were deparaffinized in Bio-Clear, rehydrated, and incubated overnight at room temperature with primary antibodies (0.5% milk, 10% fetal bovine serum, 1% bovine serum albumin in H_2O + Na-Azide 0.02%). The following antibodies were used: Mash1 (mouse, IgG1, 556604, 1:150; BD Pharmingen, San Jose, CA, USA), Pax6 (rabbit, AB5409; 1:2000; Chemicon, Billerica, MA, USA), Nkx2.1 (rabbit, sc13040, 1:1500; Santa Cruz Biotechnology, Dallas, TX, USA), and Otx2 (rabbit, ab114138, 1:10,000; Abcam, Cambridge, United Kingdom). The MACH 4 Universal HRP-Polymer Polymer Detection Kit (M4U534; Biocare Medical, Pacheco, CA, USA) was used for immunohistochemical detection. The specificity of Mash1, Pax6, Nkx2.1, and Otx2 was validated in mouse embryos and is described in detail in the Supplemental Fig. S1*B, C*.

Measurements of mRNA levels of interneuron-related genes

Mice were euthanized by decapitation at PND1, 9, 30, and 75. The brains were removed and the PFC immediately dissected and frozen on liquid nitrogen. PFC was handly dissected by performing a coronal cut with a razor blade at ~1.5-mm anterior to bregma in PND30 and PND75 mice and 0.5–1-mm anterior to bregma in PND1 and PND9 mice. We have then removed the medial portion of both hemisheres in the section anterior to the coronal cut with tissue forceps with 0.5-mm tips. The dissected tissue includes the cingulate cortex, the prelimbic and infralimbic cortex, the dorsal peduncular cortex, the medial orbital cortex, and the most medial part of the secondary motor cortex. Total RNA was extracted using the Trizol reagent (Thermo Fisher Scientific, Waltham, MA, USA) according to the manufacturer's instructions. The RNA was further treated with DNase (Qiagen, Germantown, MD, USA), and single strand cDNA was synthesized from 1.5 μg of total RNA using Superscript III (Thermo Fisher Scientific) and random hexamers. Real-time PCR was performed on 15 ng of cDNA by using specific primers and Power SYBR Green Master Mix (Bio-Rad, Hercules, CA, USA) on an Applied Biosystems Step-One instrument.

Thermal cycler conditions were as follows: 10 min at 95°C, 40 cycles of denaturation (15 s at 95°C), and combined annealing-extension (1 min at 58–60°C). Primer sequences of all genes are reported in Supplemental Table S1. mRNA copy number for each gene was calculated from serially diluted standard curves simultaneously amplified with the samples and normalized with respect to the transferrin receptor mRNA copy number. Each sample was analyzed in duplicate together with 2 negative controls.

Western blot analysis of PV, GluN1 subunit of NMDA receptors, and the K^+/Cl^- symporter

PV and GluN1 protein levels were examined in the PFC at PND30 and PND75. The K^+/Cl^- symporter (KCC2) protein levels were examined in the PFC at PND9 and PND30. Tissue was dissected out and homogenized at 4°C in a buffered solution composed of Tris-HCl pH 7.5, 10 mM; NaCl, 150 mM; SDS 10%, EDTA, 5 mM; PMSF, 10 mM; IGEPAL, 1%; leupeptin, 1 μg/ml; and aprotinin, 1 μg/ml. Equal amounts of proteins (20 μg) from supernatants were separated by 12% SDS polyacrylamide for PV protein and 8% for GluN1 and KCC2 proteins. After separation, proteins were transferred on immunoblot PVDF membranes. Membranes were incubated with the primary antibody and then incubated for 1 h with the secondary antibody anti-mouse or anti-rabbit (1:7000, peroxidase-coupled). The following primary antibodies were used: rabbit monoclonal anti-PV (ab11427, 1:2500; Abcam), mouse monoclonal anti-β-tubulin (sc-58886, 1:1000; Santa Cruz Biotechnology); rabbit polyclonal anti-KCC2 (ab49917, 1:2000; Abcam), rabbit polyclonal anti-GluN1 (ab109182, 1:5000; Abcam); and mouse monoclonal anti-β-actin (A5316, 1:50,000; MilliporeSigma, Burlington, MA, USA). Immunostaining was revealed by the enhanced ECL Western blotting analysis system (Hybond ECL; GE Healthcare, Waukesha, WI, USA) or by the Chemidoc computerized densitometer (Bio-Rad), and quantified by ImageLab 3.0 software (Bio-Rad).

Stereological cell counting of PV^+ neurons in the PFC

Brains from wild-type and mGlu3$^{-/-}$ mice at PND9 and PND30 were dissected out, fixed in Carnoy's solution (ethanol 60%, acetic acid 10%, and chloroform 30%), and included in paraffin. Tissue sections (20 μm) were incubated overnight with rabbit polyclonal anti-PV antibodies (ab11427, 1:100 at PND9; Abcam and PV27, 1:500 for PND30; Swant, Fribourg, Switzerland), and then for 1 h with secondary biotin-coupled anti-rabbit antibodies (1:200; Vector Laboratories, Burlingame, CA, USA). For detection, 3,3-diaminobenzidine tetrachloride (MilliporeSigma) was used. Control staining was performed without the primary antibodies. The number of PV^+ cells in the PFC (from +2.1 to +1.34 from bregma according to the Paxinos (43), for PND30 mice and the corresponding sections for PND9 mice) was assessed by stereological technique and optical fractionator using a Zeiss Axio Imager M1 microscope equipped with a motorized stage, a focus control system (Zeta axis), and a digital video camera (44). The software Image-Pro Plus 6.2 for Windows (Media Cybernetics, Rockville, MD, USA) equipped with a Macro was used for the analysis of digital images. Macro was obtained by Immagine and Computer (Milan, Italy). The characteristics of this Macro have been previously reported in Gundersen and Jensen (45). The analysis was performed on 4 sections of 20 μm, sampled every 220 μm in the rostrocaudal extension of the PFC (medial portion of the sections containing the cingulate cortex, the prelimbic cortex, the infralimbic cortex, and the dorsal peduncular cortex) using a grid of disectors with a counting frame of 40 × 40 μm, and a grid size (distance between disectors center to center) of 150 × 150 μm. The total number of PV^+ cells was computed according to the formula: $N = \Sigma(n) \times 1/SSF \times 1/ASF \times 1/TSF$, where n is the total number of cells counted on each disector; SSF (fraction of sections sampled) is the number of regularly spaced sections used for counts divided by the total number of sections across the areas; ASF (area sampling frequency) is the disector area divided by the area between disectors (disector area × disector number/region area); and TSF (thickness sampling frequency) is the disector thickness divided by the section thickness. The Cavalieri estimator method was used to evaluate the volume of the PFC (44).

Immunohistochemical analysis of Cat-315^+ PNNs and *Wisteria floribunda* agglutinin$^+$ PNNs

We measured the number of cortical cells enwrapped by PNNs stained by either the anti-CSPG antibody, Cat-315, or the lectin, *Wisteria floribunda* agglutinin (WFA), in the PFC or in 3 portions

of the cerebral cortex (Cat-315 and WFA) of wild-type and mGlu3$^{-/-}$ mice at PND21 and PND30. Free-floating brain slices were rinsed in PBS, quenched in 3% H_2O_2 and 10% methanol for 15 min, and blocked in 5% normal donkey serum and 0.25% triton X-100 in PBS for 1 h at room temperature. For Cat-315 staining, sections were incubated overnight at 4°C with monoclonal mouse anti-CSPG antibodies (Cat-315, Mab1581, 1:3000; MilliporeSigma) diluted in blocking solution. Following rinses with 2% normal donkey serum and 0.25% triton X-100 in PBS, sections were incubated with a donkey anti-mouse secondary antibody (1:400) for 90 min at room temperature for 3,3-diaminobenzidine tetrachloride staining. Bright-field pictures were acquired using an Olympus BX60 microscope. We also performed double immunofluorescent staining for Cat-315 and PV (with monoclonal rabbit anti-PV antibodies, 1:1000, PV27; Swant) using secondary donkey anti-mouse Alexa Fluor 488 antibody (1:200; Thermo Fisher Scientific) and donkey anti-rabbit Cy3 antibody (1:200; Jackson ImmunoResearch, Cambridge, United Kingdom). WFA fluorescent staining was performed using biotin-conjugate WFA (1:500, L1516; MilliporeSigma) and fluorescent secondary antibody (Streptavidin Alexa Fluor 488, 1:200; Thermo Fisher Scientific). Sections were examined with a Zeiss Carl Axiophot2 microscopy (Carl Zeiss, Oberkochen, Germany) and processed with NIS-elements F3.0.

For Cat-315 staining, bright-field cell counting was performed in 3 coronal sections per brain (+0.98, +0.02, and −1.06 mm relative to bregma) as previously reported in Quattromani *et al*. (46). In brief, composite micrographs of both hemispheres were acquired through a ×4 magnification objective using the CellSens Dimension Software (BX60; Olympus, Tokyo, Japan). An optical grid was used to define distances and draw the boundaries of the cortex in both hemispheres according to the Paxinos atlas (43). Cat-315$^+$ cells were counted in the whole cortical mantle and in all cortical layers of the 3 anatomical sections bilaterally at PND21 and unilaterally at PND30.

For WFA staining, cell counting was performed unilaterally in the same 3 coronal sections used for Cat-315 staining (+0.98, +0.02, and −1.06 mm from bregma), with the difference that cells were counted at ×10 magnification uniltaterally only in the rectangular areas highlighted in gray (and not in the whole cortical mantle). WFA$^+$ cells were also counted in 3 PFC sections at +1.78, +1.54, and +1.34 from bregma. In the latter sections, cell counting was performed at 10× magnification in the medial portion containing the prelimbic cortex, infralimbic cortex, and dorsal peduncular cortex in all sections, and cingulate cortex 2 in the +1.34 section.

Electrophysiological analysis of GABAergic transmission in the PFC

Cortical slices were prepared from PND9 and PND30 wild-type and mGlu3$^{-/-}$ mice. Coronal slices (350 μm) were cut in glycerol-based artificial cerebrospinal fluid (ACSF) with a vibratome (Leica VT 1000S; Leica Microsystems, Wetzlar, Germany), placed in a slices incubation chamber at room temperature with oxygenated ACSF, and transferred to a recording chamber within 1–6 h after slices preparation. Whole-cell patch-clamp recordings were performed on pyramidal neurons at 24–25°C. Membrane currents were recorded using glass electrodes (8–10 MΩ) filled with the following (in millimolars): 111 K-gluconate, 6 KCl, 0.5 $CaCl_2$, 10 HEPES, 5 BAPTA, 2 Mg-ATP; pH 7.3, with KOH. The calculated Cl^- reversal potential for our solution was −77 mV. Resting membrane potential (MP) was −64 ± −3 mV. GABA was photolyzed from bis(2,2′-bipyridine-*N*,*N*′)triphenylphosphine)-4-aminobutyric acid ruthenium hexafluorophosphate complex (RuBi GABA, ab120409; Abcam) using local uncaging as previously described in Khirug *et al*. (47). RuBi GABA (2.5 mM) was dissolved in ACSF and delivered to cells by pressure applications (1–5 ψ; Picospritzer II, General Valve) from glass micropipettes positioned above whole-cell voltage-clamped neurons. For local photolysis of caged RuBi GABA, a 476-nm laser flash (LASU System; Scientifica, Uckfield, United Kingdom) was delivered to the slice, through a LUM-PlanFl ×40 water-immersion objective (Olympus). The beam yielded an uncaging spot of ∼10 μm in diameter that was focused either at the soma or at dendrite trees at a distance of 50 μm from the soma. The laser power (10 mW at the objective output) and flash duration (10 ms) were set at a level that provided a good signal-to-noise ratio for uncaging-evoked currents. The current/voltage (I/V) relationship was determined by varying the holding potential from −80 to −30 mV (10 mV steps, 3 s long). Peak current amplitudes were plotted against the MP to measure the local reversal potential of GABA currents (E_{GABA}). The laser flash evoked no responses in the absence of RuBi GABA. Junction potential calculated for our solution was −14 mV, and MP was corrected accordingly.

Video-EEG data recording and analysis

EEG recording and analysis of data were performed in 9 mGlu3$^{-/-}$ and 9 wild-type mice. These mice were adapted to the laboratory conditions for 1–2 wk before implantation of EEG epidural electrodes. During this period, they were housed under standard conditions (see above) and received a gentle handling for about 5–10 min per day. Food and water were available *ad libitum*. Stainless steel insulated electrodes with mounting screw and socket contacts (3.2-mm screw wire length of 10 mm, E363/20/SPC; Bilaney, Kent, United Kingdom) were implanted under isoflurane (3%) anesthesia and intraperitoneal injection of rompun (20 mg/ml) at the dose of 75 mg/kg + zoletil (1 mg/ml) at the dose of 20 mg/kg. Mice were placed in a stereotaxic head frame where the exploring EEG electrodes were positioned on the *dura mater* surface overlying the anterior frontal and posterior parietal cortical regions using the following stereotaxic coordinates: AP +2.8 mm and ML at −0.5 mm from bregma for the frontal electrode; AP −2.0 mm and ML −2.0 mm for the parietal electrode, according to the Paxinos atlas (43). The exploring electrodes were referred to a reference electrode placed into the cerebellum, whereas the ground electrode was located in the nose bone. This electrode montage was successfully used for the investigation of the ongoing EEG oscillatory activities in wild-type and transgenic mice accumulating amyloid in the brain mice in the FP7 Innovative Medicine Initiative (IMI) of the European Project with the short name "PharmaCog" (48, 49). After the surgical procedure, mice were kept at a warm temperature to avoid anesthesia-induced hypothermia. A few hours after surgery, the mice were treated by systemic analgesics and antibiotics. In the week following electrode implantation, all mice experienced a period of full recovery without handling or EEG recordings. Afterward, mice received a gentle handling for about 5–10 min a day. EEG recordings started 10 d after surgery.

In any EEG experimental day, Grass Technologies 2011 (Twin software 4.5.3.23) were used for the simultaneous EEG and video digital recordings in a couple of mice (1 wild-type and 1 mGlu3$^{-/-}$ mouse). These mice were simultaneously connected to a system consisting of an AS40 Amplifier by a flexible cable. EEG data were recorded with a sampling rate of 200 Hz and an antialiasing bandpass filter (0.1–70 Hz). Nine couples of mice were used for a continuous video-EEG recording of 24 h (*i.e.*, 12 h with light on, and 12 h with light off). Any couple was formed by 1 wild-type and 1 mGlu3$^{-/-}$ mouse, each animal being free to move in a separate cage. The simultaneity of the video-EEG recording paired the effects of any environmental source of electric fields on EEG recording in a given couple of mice.

EEG recordings always started after the second hour from the beginning of light and darkness. EEG recordings failed in the wild-type mouse of the first recording day (*i.e.*, wild-type 01) and in the couple of mice of the last day (*i.e.*, wild-type 05 and

mGlu3$^{-/-}$ 05) because of technical failures (*e.g.*, bad contacts of the exploring electrodes, unexpected crashes of EEG recording system during long periods of 12 h with light off). The video recordings were used for behavioral analysis according to the procedures developed in the PharmaCog project (43, 44). In the analysis of behavioral data, we classified animal behavior during ongoing EEG recordings. Two trained experimenters (C.D.P. and M.T.P.) classified recording epochs lasting 10 s into the following behavioral classes:

1. Active behavior (condition): This kind of epoch showed animals performing overt exploratory movements in the cage for most of the given period of 10 s. The exploratory movements had to be characterized by ample displacements of body parts such as trunk, head, or forelimbs, or any combination thereof. They are not to be confounded with instinctual activities.
2. Passive behavior in wakefulness (condition): This kind of epoch showed mice exhibiting passive behavior corresponding to a substantial animal immobility for most of the given period of 10 s. To avoid a misclassification with respect to the sleep, this condition had to be characterized by short immobility or small movements of the trunk, head, or forelimbs, or any combination thereof. For the same reason, the experimenter did not score as passive behavior epochs showing mice staying continuously still for 20 s (or longer).
3. Behavioral sleep state: This kind of epoch showed mice exhibiting a sleep state from a behavioral point of view. This state corresponded to an animal immobility for a long observation period lasting several minutes. Another important sign was neck muscle relaxation when detectable in the video recordings. Particular attention was again devoted to minimizing the misinterpretation between sleep state and passive conditions.
4. Instinctual behavior: This kind of epoch showed mice exhibiting instinctual activities, such as drinking, cleaning, eating, *etc*., for most of the given period of 10 s. Special attention was paid not to include these epochs into the class denoting active behavior.
5. Undefined: This kind of epoch was characterized by a lack of clarity about the behavioral condition of the animal. Such epochs were rejected from the EEG data analysis.

For the analysis of EEG data, an EEG recording interval of 1 h was selected in the light-off condition (from 6:00 PM to 6:00 AM), corresponding to the wakefulness of the mice. The selected period had the schedule of 11:00 to 12:00 PM. Of note, this period was very far the lighting change (transition from light on to light off) to minimize effects of the stress on EEG readouts.

To avoid the confounding effects of major motor activity and sleep (we could not determine sleep stages without electrooculographic and electromyographic recordings), the EEG data analysis was only focused on behavioral epochs (lasting 10 s) related to the passive state in the wakefulness (*i.e.*, 11:00–12:00 PM). Any epoch (lasting 10 s) of the passive state was segmented into 5 consecutive EEG epochs lasting 2 s. In the periods of interest, the EEG epochs were visually inspected to identify and reject those with EEG signals contaminated by instrumental or biologic artifacts. Afterward, a standard spectral analysis of artifact-free EEG signals was performed by digital fast Fourier transform–based procedures. The analysis was focused on the spectralrange with greatest EEG power density (*i.e.*, 2–45 Hz).

For each mGlu3$^{-/-}$ or wild-type mouse, the 2-s EEG epochs were used as an input to a fast Fourier transform–based spectral analysis using Welch technique, Hanning windowing function, and no phase shift. The EEG power density was computed with 0.5 Hz of frequency resolution (script in MatLab 6.5; MathWorks, Natick, MA, USA). The relative solutions were averaged across the following frequency bands of interest that were selected: 2–7 Hz (δ-θ), 8–13 Hz (α), 14–34 Hz (β), 35–45 Hz (γ). The same procedure was followed for wild-type mice. Logarithmic transformation was applied to reduce intervariability of EEG power density values across mice. At the end of the procedure, enough artifact-free EEG epochs related to passive wake were obtained in 7 wild-type and 8 mGlu3$^{-/-}$ mice. Data analysis of EEG power density values was performed in those mice.

Finally, we performed a control analysis to test the hypothesis that in wild-type mice, the general EEG spectral features in the period of interest (*i.e.*, 11:00–12:00 PM) did not differ from those of other periods of interest in the light off condition (from 6:00 PM to 6:00 AM), which are mainly characterized by wakefulness. To this aim, we considered 2 additional control periods, namely from 8:00 to 9:00 PM (P1) and from 9:00 to 10:00 PM (P2). In this line, we named the period of interest from 10:00 to 11:00 PM as P3. In a first step of the analysis, we selected the wild-type mice having enough artifact-free EEG epochs related to passive wake in the 3 periods of interest ($n = 7$). In a second step, the EEG power density of the artifact-free 2-s EEG epochs were compared among P1, P2, and P3 in the mentioned frequency bands (*i.e.*, 2–7, 8–13, 14–34, and 35–45 Hz).

Statistical analysis

Statistical analysis of biochemical data, immunohistochemical data, and electrophysiological data of GABAergic transmission were carried out by either Student's *t* test or 1-way ANOVA followed by Fisher's least significant difference (LSD). Statistical analysis of EEG data was performed by Statistica 10.0 packages (StatSoft, Tulsa, OK, USA; *www.statsoft.com*). An ANOVA ($P < 0.05$) used EEG power density as a dependent variable. ANOVA factors were the 2 genotypes (wild-type and mGlu3$^{-/-}$ mice) and the frequency bands (2–7, 8–13, 14–34, and 35–45 Hz). The Duncan test was used as *post hoc* test for planned comparisons. Finally, an ANOVA ($P < 0.05$) evaluated the control hypothesis that in the wakefulness day period, EEG oscillations did not differ as general spectral features in 3 distinct periods lasting 1 h (*i.e.*, P1, P2, and P3) in the wild-type group. The ANOVA-dependent variable for the analysis was the mean of the EEG power density in the frontal-parietal electrode montage. ANOVA factors were as follows: time (P1, P2, and P3) and frequency bands (2–7, 8–13, 14–34, and 35–45 Hz). The Duncan test was used for *post hoc* comparisons.

RESULTS

Genetic deletion of mGlu3 receptors lowers the expression of biochemical markers of cortical interneurons during postnatal development

We first examined whether the expression of genes that determine the fate of GABAergic interneurons in the embryonic life was influenced by genetic deletion of either mGlu2 or mGlu3 receptors. Mash1 is a bHLH transcription factor that is expressed in proliferative zones of the forebrain and is required for neuronal differentiation (50–52). Otx2 has a key role in the specification of thalamic GABAergic interneurons (53) and in the postnatal maturation of PV^{+} cortical interneurons (54–57). Pax6 is a paired-box transcription factor, which is expressed by progenitor cells in the ventricular zone of the dorsal telencephalon and regulates the number and migration of

GABAergic interneurons in the embryonic life (58, 59). The transcription factor, Nkx2.1, which is expressed in the medial ganglionic eminence of the telencephalon, has a key role in specification of GABAergic interneurons (60–63). Immunostainig performed in embryos at E12.5 did not show apparent changes in the expression pattern of Pax6, Otx2, Mash1, and Nkx2.1 in either mGlu2$^{-/-}$ or mGlu3$^{-/-}$ mice (Supplemental Fig. S1*A*).

We next examined whether the lack of mGlu2 or mGlu3 receptors could affect the expression of genes encoding for biochemical markers of GABAergic interneurons in the PFC in the first month of postnatal life. At PND1, both mGlu2$^{-/-}$ and mGlu3$^{-/-}$ mice showed a reduction in the transcripts encoding for somatostatin (Sst), vasoactive intestinal peptide (VIP), and the α_5 subunit of $GABA_A$ receptors. mGlu3$^{-/-}$ differed from mGlu2$^{-/-}$ mice in the expression of the transcripts encoding for the transcription factor aristaless (Arx), α5 subunit of GABAA receptors, and neuropeptide Y (NPY), and Reelin. Arx and CB1 mRNA levels were selectively reduced in mGlu3$^{-/-}$ mice and NPY mRNA levels were significantly reduced in mGlu2$^{-/-}$ mice and increased in mGlu3$^{-/-}$ mice, whereas Reelin mRNA levels were selectively increased in mGlu3$^{-/-}$ mice as compared with wild-type mice (**Fig. 1*A***). PV mRNA levels were undetectable at PND1.

At PND9, PV mRNA levels could be detected in PFC and were differentially regulated by mGlu2 and mGlu3 receptors. PV mRNA levels were substantially reduced in mGlu3$^{-/-}$ mice and increased in mGlu2$^{-/-}$ mice (Fig. 1*A*). The transcripts encoding for GluN1 and NPY were reduced in mGlu3$^{-/-}$ mice. CB1 receptor and $GABA_A$ δ subunit mRNA levels were reduced in both mGlu2$^{-/-}$ and mGlu3$^{-/-}$ mice (Fig. 1*A*).

At PND30, only a few transcripts were affected by the lack of mGlu2 or mGlu3 receptors. Interestingly, mGlu3$^{-/-}$ mice showed a robust reduction in PV mRNA levels, a reduction in GluN1 subunit, and an increase in carletinin and Reelin mRNA levels. mGlu2$^{-/-}$ mice only showed a reduction in PV mRNA levels (Fig. 1*A*).

We also measured PV and GluN1 protein levels at PND30 (PV protein levels were undetectable by Western blot analysis at PND9). A significant reduction in PV and GluN1 protein levels was found in mGlu3$^{-/-}$ mice at PND30 (Fig. 1*B*).

In a separate set of experiments, we extended the analysis of selected transcripts and PV and GluN1 protein levels to adult mice (PND75). The analysis was exclusively carried out in mGlu3$^{-/-}$ mice and their wild-type counterparts. As observed at PND30, adult mGlu3$^{-/-}$ mice showed a significant reduction in PV and GluN1 protein levels in the PFC. However, mRNA levels of PV, GluN1, Sst, glutamate decarboxylase (Gad)-67 (Gad1), Gad-65 (Gad2), and Reelin did not differ between mGlu3$^{-/-}$ and wild-type mice at PND75 (Fig. 2*A*, *B*).

These findings suggest that the lack of mGlu3 receptors causes an abnormal development of PV$^+$ GABAergic interneurons in PFC. To exclude that the observed biochemical changes could reflect alterations in the absolute number of interneurons, we also performed a stereological counting of PV$^+$ neurons in the PFC at PND9 and PND30. The absolute number of PV$^+$ interneurons did not differ between mGlu3$^{-/-}$ mice and their wild-type counterparts at both ages (Supplemental Fig. S2*A*–*C*).

Changes in Cat-315$^+$ and WFA$^+$ PNNs in the cortex of mGlu3$^{-/-}$ mice

We also examined whether the lack of mGlu3 receptors could affect the density of Cat-315$^+$ and WFA$^+$ PNNs at PND21 and PND30. In a first set of experiments, we measured the density of PNNs labeled by the CSPG Cat-315 antibody in mGlu3$^{-/-}$ mice and their wild-type counterparts at PND21 and PND30. Cat-315 immunostaining was faint in the PFC, and, therefore, we carried out the analysis in the cerebral cortex at 3 levels corresponding to +0.98, +0.02, and −1.06 mm from bregma. These portions of the cortex are posterior to the PFC and contain the primary and secondary motor cortex and different subregions of the somatosensory cortex in addition to area 1 and area 2 of the cingulate cortex (+0.98 and +0.02 mm from bregma) and the retrosplenia cortex (−1.06 mm from bregma). Double immunofluorescence showed that most of the neurons enwrapped by Cat-315$^+$ PNNs at PND21 were PV$^+$ (**Fig. 3*A***). An increased density of Cat-315$^+$ PNNs was found in the cerebral cortex of mGlu3$^{-/-}$ mice at PND21, but not at PND30 (Fig. 3*A*–*C*). For the evaluation of PNNs in the PFC, we performed staining for the lectin WFA, which labels *N*-acetylgalactosamines-β1 present in PNNs (64). The density of WFA$^+$ PNNs was also significantly increased in the PFC at PND21, but not at PND30 (**Fig. 4*A*–*D***). We could also confirm the increased density of PNNs in the 3 posterior regions of the cerebral cortex by WFA staining (Fig. 4*E*–*H*).

Cortical pyramidal neurons from PND9 mGlu3$^{-/-}$ receptor mice exhibit depolarized E_{GABA}

The shift of $GABA_A$ receptor function from excitatory to inhibitory in the early postnatal life represents a key event in the developmental trajectory of the CNS. To examine whether the lack of mGlu3 receptors could affect this process, we evaluated E_{GABA} in L5 pyramidal neurons (exhibiting the usual firing profile; **Fig. 5*A***) of PFC from wild-type and mGlu3$^{-/-}$ mice, in both somata and apical dendrites, by means of uncaging GABA experiments (47, 65). In PND9 wild-type mice, laser flashes applied to the soma (Fig. 5*B*) evoked GABA currents (I_{GABA}) in whole-cell I_{GABA} with an E_{GABA} of −78 ± 1 mV (Fig. 5*C*; n = 11; in agreement with the calculated E_{Cl}, −77 mV); in PND9 mGlu3$^{-/-}$ mice the E_{GABA} values were −74 ± 1 mV (Fig. 5*D*, *E*; n = 10; P = 0.033), indicating a less efficient Cl^- extrusion in mGlu3$^{-/-}$ mice at this age. No difference was found between E_{GABA} values measured in the apical dendrites of the same cells: −74 ± 2 and −75 ± 1 mV for wild-type and mGlu3$^{-/-}$ mice, respectively (Fig. 5*E*). Because expression of the K^+-Cl^- antiporter, KCC2, drives developmental changes in Cl^- homeostasis and E_{GABA} in neurons (66), we also examined KCC2 protein levels by immunoblotting in the PFC of wild-type and mGlu3$^{-/-}$ mice. Interestingly, KCC2

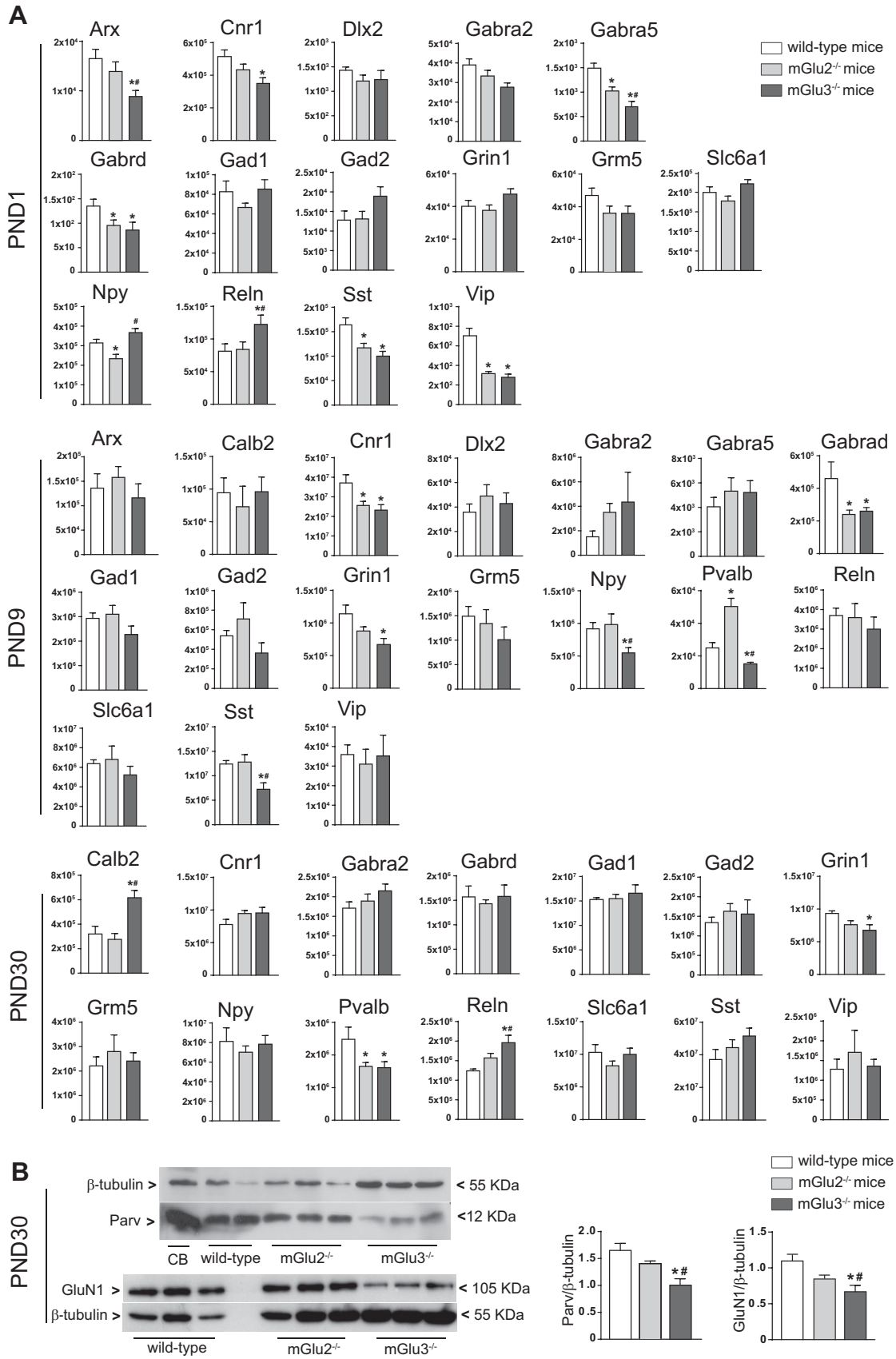

Figure 1. Influence of genetic deletion of mGlu2 or mGlu3 receptors on biochemical markers of GABAergic interneurons in the PFC during postnatal development. *A*) Changes in the transcript of interneuron-related genes at PND1, -9, and -30. Gene nomenclature is used in the figure. mRNA values, expressed as copy number, were normalized to transferrin receptor (TFRC)

(*continued on next page*)

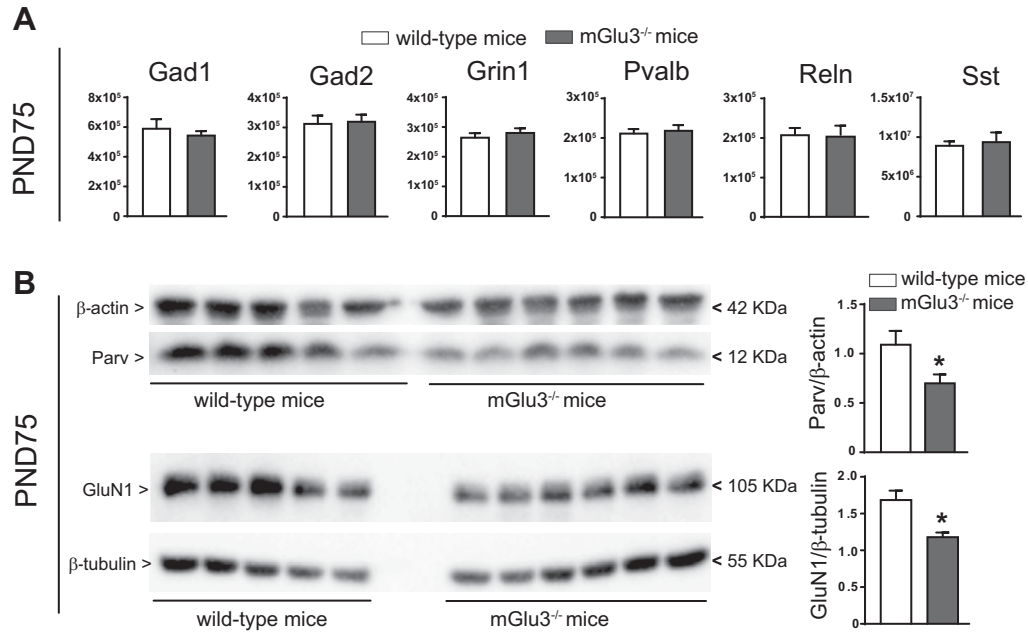

Figure 2. Analysis of selected transcripts and protein levels of interneuron-related genes in wild-type and mGlu3$^{-/-}$ mice at PND75. *A*) mRNA levels of PV, GluN1 subunit of NMDA receptors (Grin1), Sst, Gad1, Gad2, and Reelin (Reln) genes (see Fig. 1 for the corresponding proteins); *B*) Immunoblot analysis of PV and GluN1. Values are means ± SEM of 5–6 mice/group. *Statistically significant (Student's *t* test) *vs.* wild-type mice. Parv: $t_9 = 2.69$; $P = 0.0248$; GluN1: $t_9 = 4.104$; $P = 0.00266$.

protein levels were significantly reduced in mGlu3$^{-/-}$ mice (Fig. 5*F*), which is in close agreement with the more depolarized E_{GABA} found in these animals.

L5 pyramidal neurons from mGlu3$^{-/-}$ mice at PND30 showed less depolarized dendritic E_{GABA}

At PND30, somatic E_{GABA} in wild-type mice was similar to that recorded at PND9 (-76 ± 1 *vs.* -78 ± 1 mV $P = 0.374$). This was not unexpected because most of the developmental increase in KCC2 expression in the mouse cerebral cortex occurs in the first 2 wk of postnatal life (67, 68). E_{GABA} values did not differ between wild-type and mGlu3$^{-/-}$ mice at PND30 (-76 ± 1 mV and -77 ± 1 mV, $n = 9$ and $n = 10$, respectively; Fig. 5*G*; $P = 0.365$), indicating a recovery of Cl^- extrusion in mGlu3$^{-/-}$ mice after weaning. At this age, however, E_{GABA} measured in dendrites was significantly more negative in mGlu3$^{-/-}$ mice than in their wild-type counterparts (-77 ± 1 *vs.* -73 ± 1 mV, respectively; Fig. 5*H, I*; $P = 0.036$), suggesting a lower subcellular heterogeneity of Cl^- transport in mGlu3$^{-/-}$ L5 pyramidal neurons. In apparent contrast with data obtained at PND9, mGlu3$^{-/-}$ mice at PND30 showed a substantial increase in KCC2 protein levels in the PFC (Fig. 5*J*).

Influence of mGlu3 receptors on EEG oscillatory activity in adult mice

Figure 6*A* shows frontal-parietal EEG power density values in wild-type mice in 3 time intervals lasting 1 h (P1: 8:00–9:00 PM; P2: 9:00–10:00 PM; P3: 11:00–12:00 PM) during the light-off period (from 6:00 PM to 6:00 AM). Mice were mainly awake during these time intervals. All artifact-free 2-s EEG epochs were considered. The frequency bands of interest were 2–7, 8–13, 14–34, and 35–45 Hz. Of note, background levels of frontal-parietal EEG power density across all frequency bands did not differ among P3 (the time interval used for the comparative analysis between wild-type and mGlu3$^{-/-}$ mice), P1, and P2. ANOVA confirmed the lack of difference and the general reliability of the EEG spectral features in our experimental design.

Figure 6*B* shows the EEG power density computed from the bipolar frontal-parietal electrode montage in adult wild-type and mGlu3$^{-/-}$ mice. Input data from the spectral analysis referred to the animal passive behavioral state observed in the quiet wakefulness. The EEG power

and are means ± SEM of 5–9 mice/group. Statistical analysis was performed by 1-way ANOVA + LSD. Statically significant *vs.* the corresponding values of wild-type (WT) (*) or mGlu2$^{-/-}$ (#) mice are reported in Supplemental Table S2. *B*) Western blot analysis of PV and the GluN1 subunit of NMDA receptors in the PFC at PND30. Densitometric values are means ± SEM of 6–10 mice per group. Representative blots are shown. Calb2, carletinin; CB, cerebellum from adult mice, used as positive control for Parv expression; Cnr1, CB1 receptor; Gabra2, Gabra5, and Gabrd, α_2, α_5, and δ subunits of $GABA_A$ receptors; Grin1, GluN1 subunit of NMDA receptors; Grm5, mGlu5 receptor; Reln, Reelin; Slc6a1, GAT-1. 1-way ANOVA + Fisher's LSD. $P < 0.05$ *vs.* the corresponding values of wild-type (*) or mGlu2$^{-/-}$ (#) mice. *F* and *P* values are reported in Supplemental Table S2.

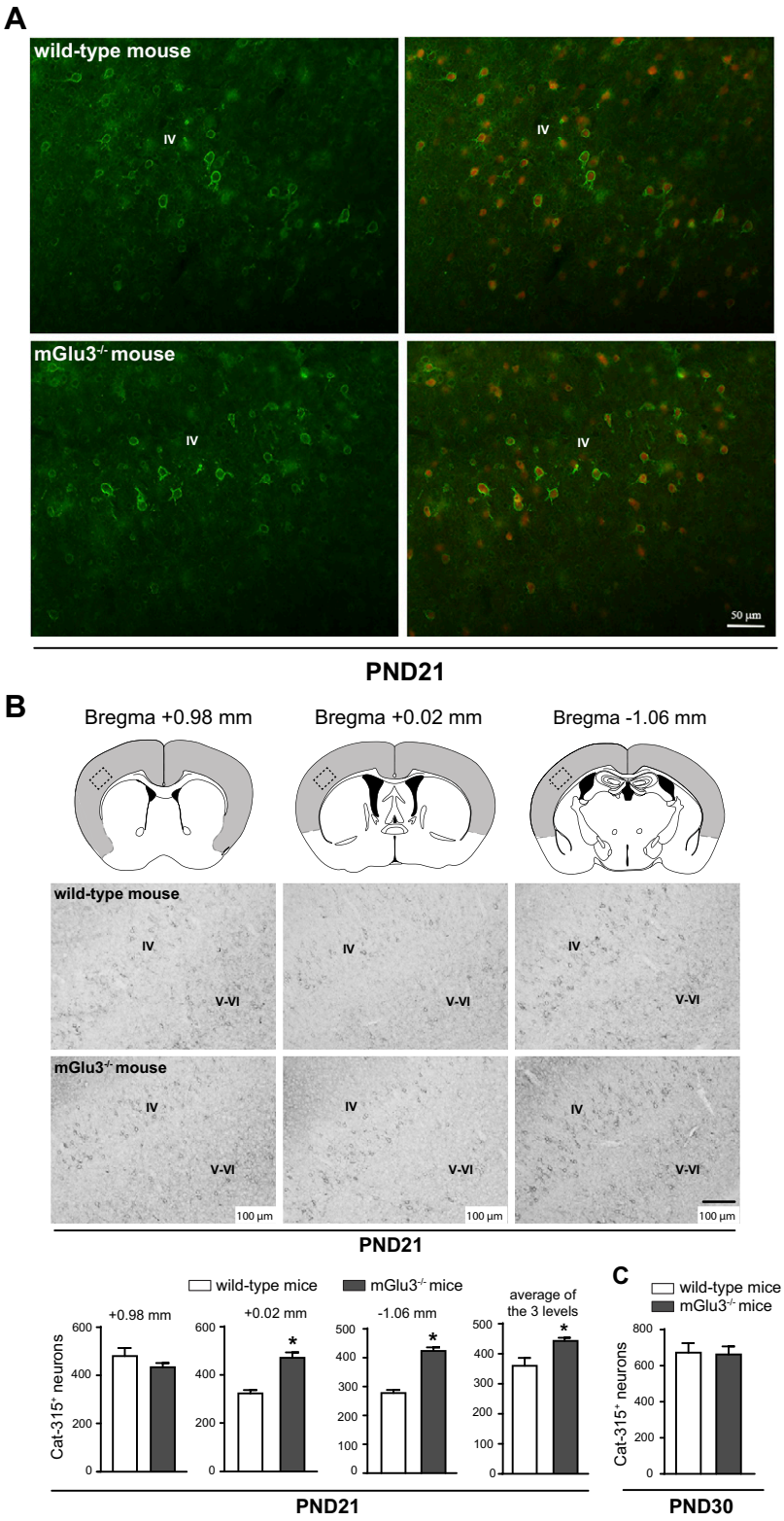

Figure 3. Increased density of Cat-315$^+$ PNNs in the cerebral cortex of mice lacking mGlu3 receptors at PND21. *A*) Double fluorescent staining for Cat-315 (green) and PV (red) in the cerebral cortex of wild-type and mGlu3$^{-/-}$ mice (at +0.02 mm from bregma). Note that the majority of neurons surrounded by Cat-315$^+$ PNNs are PV$^+$. *B*) The number of Cat-315$^+$ cells was determined in the cerebral cortex at different distances from bregma (+0.98, +0.02, and −1.06 mm). Cat-315$^+$ cells were counted bilaterally in the whole cortical mantle highlighted in gray and in all cortical layers in the 3 sections. Representative images of Cat-315 immunostaining (*B*) refer to the 3 portions of the somatosensory cortex included in the dashed rectangles. Cortical layers are indicated (*A*, *B*). Counts of Cat-315$^+$ cells in each anatomic section and average counts in the 3 sections are also shown (*B*). Values are means ± SEM of 5 mice/group *Statistically significant (Student's *t* test) *vs.* the respective values obtained in wild-type mice. +0.02 mm from bregma: $t_8 = -6.27$; $P = 0.00024$; −1.06 mm from bregma: $t_8 = -9.7$; $P = 0.00001$; average number of the 3 anatomic levels: $t_8 = 6.54$; $P = 0.0002$. *C*) Average number of neurons counted in cerebral cortex at +0.98, +0.02, and −1.06 mm from bregma in wild-type and mGlu3$^{-/-}$ mice at PND30. Cat-315$^+$ cells were counted only in 1 hemisphere. Values are means ± SEM of 3 mice/group.

density is shown at the frequency bands of 2–7, 8–13, 14–34, and 35–45 Hz. Interestingly, mGlu3$^{-/-}$ mice showed a substantial reduction in the magnitude of EEG power densities across all frequency bands as compared with wild-type mice (Fig. 6*B*). ANOVA revealed a 2-way interaction between genotypes and frequency bands ($F = 10.6$; $P < 0.01$). The planned Duncan *post hoc* analysis showed a significant difference in the magnitude of frontal-parietal EEG power density between mGlu3$^{-/-}$ and wild-type mice.

DISCUSSION

At least 4 major events occurring early after birth contribute to shape the developmental trajectory of inhibitory

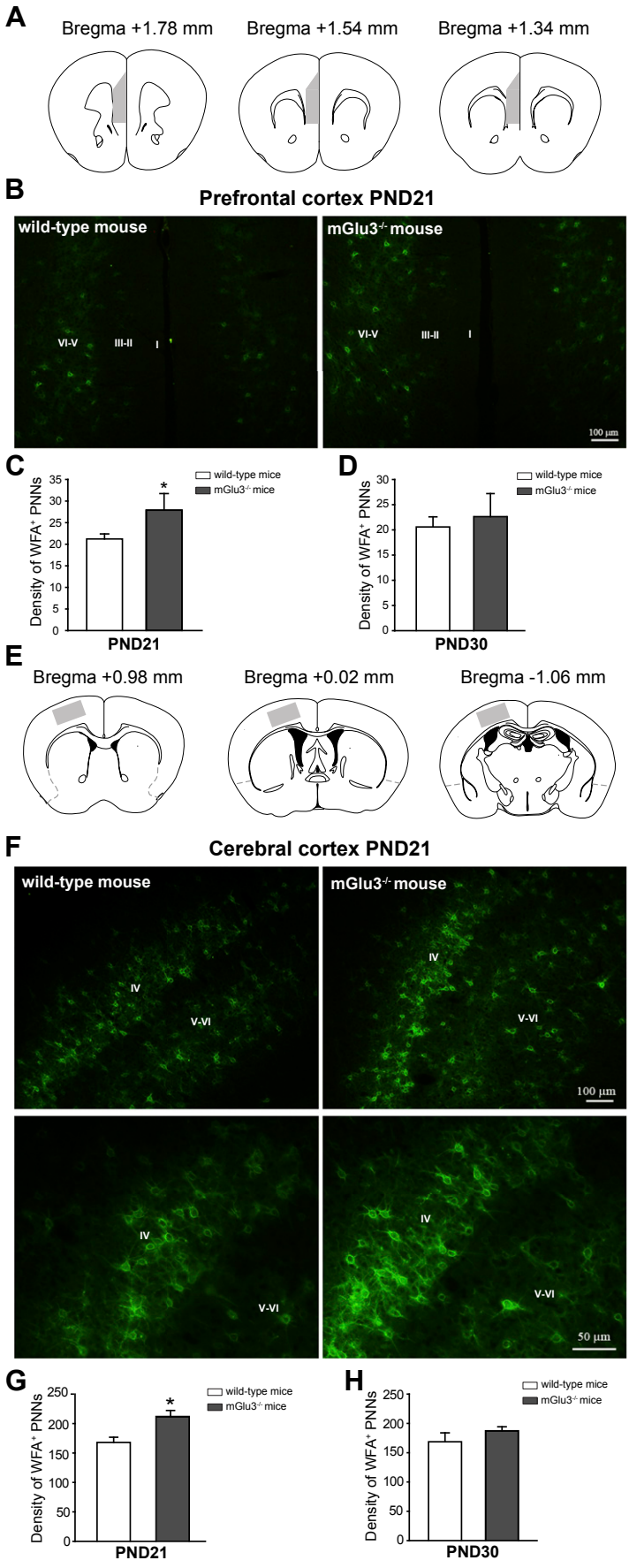

Figure 4. Increased density of WFA$^+$ PNNs in the cerebral cortex of mGlu3$^{-/-}$ mice at PND21. *A*) Fluorescent WFA staining of PNNs was performed in the medial portion of 3 sections containing the PFC (+1.78, +1.54, and +1.34 mm from bregma). Cell counting was performed at original magnification ×10 uniaterally in the portions highlighted in gray. *B*) Representative images of wild-type and mGlu3$^{-/-}$ mice at PND21 in the section at +1.54 from bregma, where cortical layers are indicated. *C*, *D*) Average density values of WFA$^+$ PNNs in the PFC of the 3 sections at PND21 and PND30, respectively. Values are means ± SEM of 3 mice/group in both graphs. *Statistically significant (Student's *t* test) *vs.* the respective wild-type mice; $t_4 = -2.87$; $P = 0.045$. *E*) WFA$^+$ cells were also counted unilaterally in the highlighted portions of the cerebral cortex in 3 sections at +0.98, +0.02, and −1.06 mm from bregma. *F*) Representative images at +0.02 mm from bregma, where cortical layers are also indicated. *G*, *H*) Average density values of WFA$^+$ PNNs in the cerebral cortex at PND21 and PND30, respectively. Values are means ± SEM of 4 mice/group at PND21 and 3 mice/group at PND30. *Statistically significant (Student's *t* test) *vs.* the respective wild-type mice; $t_6 = -6.514$; $P < 0.001$.

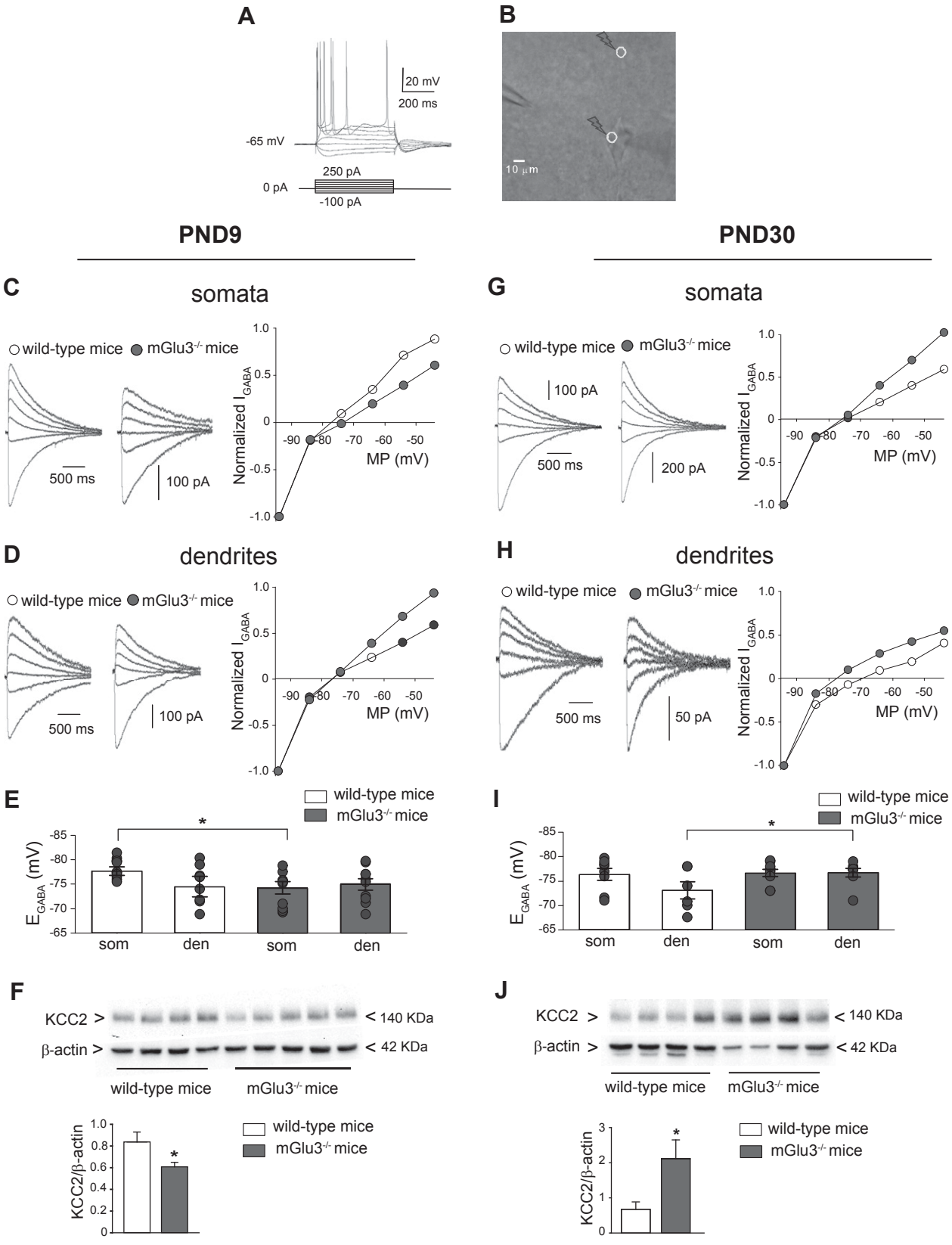

Figure 5. Effect of genetic deletion of mGlu3 receptors on $GABA_A$ receptor–mediated responses in pyramidal neurons of the PFC during postnatal development. *A*) Typical current-clamp recording of action potentials from an L5 pyramidal neuron in a slice obtained from the PFC. *B*) A microscopic image illustrating a RuBi GABA uncaging experiment, where circles represent the somatic (som) and dendritic (den) areas where laser-induced photostimulation was applied. *C, D, G, H*) Typical whole-cell I_{GABA} currents elicited by photolysis of RuBi GABA at different holding potentials and normalized *I-V* curves in som and den (about 50 μm from soma) from wild-type and mGlu3$^{-/-}$ mice at PND9 (*C, D*) and PND30 (*G, H*). *E, I*) Som and den E_{GABA} values in

(*continued on next page*)

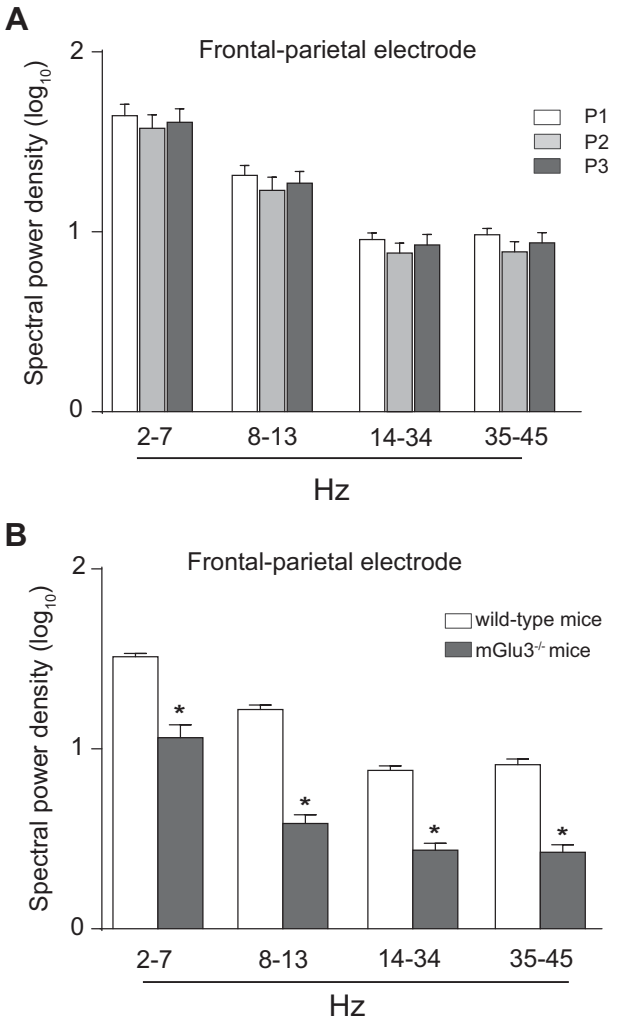

Figure 6. Effect of genetic deletion of mGlu3 receptors on EEG oscillatory activity in adult mice. *A*) Frontal-parietal EEG power density values in wild-type CD1 mice recorded in 3 time periods lasting 1 h (P1 = 8:00–9:00 PM; P2 = 9:00–10:00 PM; and P3 = 11:00–12:00 PM) in the light-off condition. All artifact-free 2-s EEG epochs were considered for the computation of those values. The frequency bands of interest were 2–7 Hz (δ-θ), 8–13 Hz (α), 14–34 Hz (β), and 35–45 Hz (γ). Values are means ± SEM of 7 mice. EEG power densities did not differ in the 3 time periods. *B*) EEG power density recorded in adult wild-type ($n = 7$) and mGlu3$^{-/-}$ ($n = 8$) mice during the P3 period. The data refer to ongoing EEG oscillations recorded during passive behavioral state in the quiet wakefulness. Values are means ± SEM. *Statistically significant *vs.* the respective values obtained in wild-type mice (1-way ANOVA + Duncan *post hoc* test). Genotype × frequency band interaction: $F = 10.6$; $P < 0.01$. *P* values (Duncan test): 2–7 Hz: $P = 0.025$; 8–13 Hz: $P = 0.001$; 14–34 Hz: $P = 0.004$; 35–45 Hz: $P = 0.001$.

GABAergic transmission in the cerebral cortex: *1*) the postnatal maturation of GABAergic interneurons, which acquire specific peptide-protein markers; *2*) the correct matching between pyramidal neurons and GABAergic interneurons (69); *3*) the GABA shift (*i.e.*, the developmental changes in neuronal chloride homeostasis driven by KCC2) (21); and *4*) the formation of PNNs, which restrain the plasticity of PV$^+$ interneurons and other neuronal types (70). Our data support the involvement of mGlu3 receptors in at least 3 of these mechanisms.

mGlu3$^{-/-}$ mice showed large reductions in the expression of PV and the GluN1 subunit of NMDA receptors, which lasted until the adult life (PND75). PV is a calcium-binding protein expressed by basket and chandelier cells, which innervate the soma and initial axonal segment of pyramidal neurons (71). NMDA receptors are highly expressed and constitutively active in PV$^+$ cells and other interneurons because the relatively low MP relieves the Mg^{2+} blockade of the ion channel (72). mGlu3$^{-/-}$ mice also showed a reduction in the transcripts encoding for VIP, Sst, and CB1 receptors at both PND1 and PND9. VIP is a specific marker of a subpopulation of interneurons that exclusively innervate other interneurons (73). Sst is a marker of Martinotti's cells that innervate the apical portion of pyramidal cell dendrites (74, 75). CB1 receptors are found in a subpopulation of PV$^-$ and cholecystokinine (CCK)$^+$ basket cells, which exhibit moderate accommodating firing patterns (76). Thus, it appears that the absence of mGlu3 receptors impairs the development of multiple populations of cortical GABAergic neurons. The reduction in Arx mRNA levels found in mGlu3$^{-/-}$ mice at PND1 is consistent with this hypothesis because Arx is essential for the development of cortical interneurons (77). We have also found that the transcript encoding for Reelin was up-regulated in the PFC of mGlu3$^{-/-}$ mice at PND1 and PND30. Reelin, a glycoprotein secreted from Cajal-Retzius cells in the embryonic life and from a subpopulation of GABAergic interneurons in the postnatal life, regulates neuronal migration in the developing cerebral cortex (78). Abnormalities in Reelin signaling are associated with psychiatry disorders (79), and a reduced expression of Reelin resulting from gene hypermethylation has been found in the brain of individuals affected by schizophrenia (80). Our data suggest that endogenous activation of mGlu3 receptors restrains Reelin expression in specific time windows during postnatal development, raising the attractive possibility that mGlu3 receptors are also involved in the regulation of neuronal migration.

The biochemical scenario of mGlu3$^{-/-}$ mice is similar to that observed in cortical tissue of individuals affected by schizophrenia, in which expression of PV, NMDA receptors, CCK, CB1 receptors, and other markers of GABAergic interneurons is consistently reduced without apparent changes in neuronal number (81–84). A reduced expression of NMDA receptors might be a primary event that drives other changes observed in mGlu3$^{-/-}$ mice.

wild-type and mGlu3$^{-/-}$ mice at PND9 (*E*) and PND30 (*I*). Values are means ± SEM of 6–9 determinations/group (obtained from 3 wild-type and 3 mGlu3$^{-/-}$ mice). Statistical analysis was performed by Student's *t* test by comparing E_{GABA} values recorded in the somata and in the dendrites separately. *Statistically significant *vs.* wild-type mice. PND9: $t_{19} = 2.295$; $P = 0.033$; PND30: $t_{11} = 2.946$; $P = 0.032$. *F, J*) Western blot analysis of KCC2 protein levels in the PFC of wild-type and mGlu3$^{-/-}$ mice at PND9 (*F*) and PND30 (*J*). Values are means ± SEM of 4–5 mice/group. Statistically significant *vs.* wild-type mice (Student's *t* test); $t_7 = 2.85$ (*F*); $P = 0.0245$; $t_6 = -2.569$; $P = 0.0424$ (*J*).

Accordingly, targeted deletion of the GluN1 subunit of NMDA receptors in cortical interneurons causes a reduced expression of GAD67 and PV, disinhibition of pyramidal neurons, and reduced synchrony in their activity and generation of EEG signals (85).

Another interesting finding was that KCC2 levels were reduced in the PFC of mGlu3$^{-/-}$ mice at PND9, and, consequently, the E_{GABA} measured in the soma of pyramidal neurons was more depolarized in these mice. $GABA_A$ receptors form Cl^--permeable ion channels that can either drive Cl^- influx or efflux depending on intracellular Cl^- concentrations. In the prenatal life, activation of $GABA_A$ receptors gives raise to excitatory postsynaptic potentials owing to the high intracellular levels of Cl^- in neurons. Expression of KCC2 in postnatal neurons lowers intracellular Cl^- concentrations, and activation of $GABA_A$ receptors leads to Cl^- influx, thereby mediating the inhibitory action of GABA in the mature brain. The more depolarized E_{GABA} found in the soma of pyramidal neurons of mGlu3$^{-/-}$ mice at PND9 suggests that, at this age, a dysfunction of PV^+ or CKK^+ interneurons, or both, may cause a down-regulation of KCC2 in their postsynaptic innervation territory in pyramidal neurons. Interestingly, KCC2 expression is reduced in the dorsolateral PFC of individuals affected by schizophrenia (86), and 1 rare loss-of-function variant of KCC2 (R952H) has been associated with schizophrenia (87). In addition, the developmental switch in $GABA_A$ receptor function is disrupted in 22q11.2 deletion syndrome, which is associated with high incidence of schizophrenia (88).

We were surprised to find that opposite changes (*i.e.*, a less depolarized E_{GABA}) were observed in dendrites of pyramidal neurons of mGlu3$^{-/-}$ mice at PND30, when an increase in PFC of KCC2 protein levels was also observed. Dendrites of pyramidal neurons are innervated by slow-spiking GABAergic interneurons, including Sst^+ interneurons. A less depolarized E_{GABA} in pyramidal neurons might further disrupt the balance between excitation and inhibition in the PFC of mGlu3$^{-/-}$ mice.

Postnatal maturation of PV^+ neurons is associated with the progressive build-up of PNNs, which are formed by a linear nonsulfated hyaluronic acid polymer joined to CSPGs through a series of linking proteins (22). PNNs enwrap about 15% of forebrain neurons, the majority of which are PV^+ (23, 24). In a first set of experiments, we stained PNN with Cat-315 antibodies, which binds to the human natural killer-1 (HNK-1) glycan epitope on aggrecan (23, 89, 90). The number of Cat-315^+ PNNs was higher in 3 sections of the cerebral cortex of mGlu3$^{-/-}$ mice at PND21, when PNNs begin to be fully expressed in the mouse cortex (25), but not at PND30. We failed to detect cells stained by Cat-315 antibodies in the PFC. For these reasons, we extended the analysis to PNNs stained with WFA. The lectin, WFA, binds to the chondroitin sulfate chains of aggrecan and is widely used to detect PNNs (91, 92). Cat-315 and WFA label distict subpopulations of PNNs (93). We could detect a small number of WFA^+ PNNs in the PFC, which was greater in mGlu3$^{-/-}$ mice at PND21. The density of WFA^+ PNNs was also greater in the 3 sections of the cerebral cortex used for the detection of Cat-315^+ PNNs in mGlu3$^{-/-}$ mice at PND21. Thus, the lack of mGlu3 receptors increased the number of 2 subsets of PNNs respectively labeled by Cat-315 and WFA at PND21, but not at PNF30. PNN deposition ensures structural stability of neuronal circuits encoding for long-term memory (26), and a reduction of PNNs have been found to improve cognitive flexibility (94, 95). Thus, an optimal level of PNNs within the appropriate time windows may be essential for the correct balance between excitation and inhibition underlying cognitive function. Our findings suggest that genetic dysfunction of mGlu3 receptors may enhance PNN formation and restrain the plasticity of PV^+ interneurons in advance with respect to the appropriate developmental time.

How might mGlu3 receptors affect the postnatal development of cortical GABAergic transmission? Traditionally, the mGlu3 receptors have been considered as presynaptic receptors that negatively modulate neurotransmitter release (3). However, electron microscopy data have shown that mGlu3 receptors are concentrated in postsynaptic elements in the PFC (96) and are involved in mechanisms of activity-dependent synaptic plasticity underlying PFC-dependent cognitive functions (97). Polymorphic variants of GRM3 in humans are associated with low performance in PFC-dependent cognitive tasks (98, 99). mGlu3 receptor activation enhanced mGlu5 receptor–mediated Ca^{2+} mobilization in PFC pyramidal neurons, and mGlu3 receptor-dependent LTD in the PFC required the endogenous activation of mGlu5 receptors (15). It is possible that the lack of mGlu3 receptors causes a primary dysfunction in pyramidal neurons, which alters the excitatory control of GABAergic interneurons. Alternatively, an interaction between mGlu3 and mGlu5 receptors may also take place in interneurons, regulating mechanisms that are essential for their development. mGlu3 receptors present in glial cells might also contribute to the development of cortical interneurons. In astrocytes, mGlu3 receptor activation stimulates the production of glial cell line–derived neurotrophic factor (100, 101), which is involved in the early development of GABAergic interneurons (102, 103). Which of the above mechanisms contributes to the regulation of Cat-315^+ and WFA^+ PNN formation in the cerebral cortex is unknown. It is possible that endogenous activation of mGlu3 receptors in neurons or astrocytes modulates the expression of enzymes involved in the formation or degradation, or both, of PNNs. This attractive hypothesis warrants further investigation.

We also performed EEG experiments in mGlu3$^{-/-}$ and wild-type mice to examine whether genetic deletion of mGlu3 receptors may have a permanent effect on neuronal synchronization and desynchronization mechanisms regulating brain arousal in quiet wakefulness. This behavioral mode is reliably detectable in mice when compared with phases of active exploration of the cage, instinctual movements, or sleep. Results of these experiments showed that the power of frontal-parietal EEG oscillations in a wide frequency range from δ to γ (2–45 Hz) was markedly reduced in mGlu3$^{-/-}$ mice as compared with their wild-type counterparts. Because of the novelty of our EEG data obtained in mGlu3$^{-/-}$ mice, and because of the lack of intracerebral recording of local field potentials from the thalamus and other relevant subcortical

structures of the ascending reticular activating systems, the interpretation of these findings can only be speculative and relies on the following observations reported in previous investigations:. cortical EEG oscillations are sustained by a corticothalamic-cortical loop, in which GABAergic neurons of the RTN regulate the firing rate of thalamocortical neurons by influencing the inactivation kinetics of T-type voltage-sensitive Ca^{2+} channels with effects on cortical EEG rhythms from δ to σ frequencies (<14 Hz) in the sleep-wake cycle (104–107). In this loop, mGlu3 receptors are present in RTN neurons (16), and were found in excitatory and inhibitory presynaptic terminals of ventrobasal thalamic nuclei (17); and network activity in the cerebral cortex is shaped by cortical interneurons and their reciprocal connections with pyramidal neurons. Specifically, pyramidal neurons and PV^+ interneurons (mainly basket cells) generate γ oscillation through the pyramidal interneuron network γ model in which asynchronously firing pyramidal neurons excite PV^+ interneurons, which, in turn, silence pyramidal neurons. Synchronous decay of inhibition allows the coordinated firing of a large group of pyramidal neurons, which, in turn, excite PV^+ interneurons giving rise to oscillatory activity in the γ frequency band (82). Because inhibitory postsynaptic currents mediated by $GABA_A$ receptors at synapses between CCK-containing basket cells and pyramidal neurons have a slow decay, it is believed that CCK^+ interneurons are mainly involved in the generation of θ oscillations (108, 109). Thus, the lack of mGlu3 receptors at different synapses at both cortical and thalamic levels may explain the reduced frontal-parietal EEG oscillations found in $mGlu3^{-/-}$ mice. A life-long dysfunction of NMDA receptors (suggested by the reduced expression of the GluN1 subunit at PND75), which mediate synaptic excitation at multiple poopulations of cortical interneurons, might also contribute to EEG changes found in $mGlu3^{-/-}$ mice.

Our findings give impetus to future studies testing the hypothesis that the reported EEG alterations might be related to the psychotic-like phenotype exhibited by $mGlu3^{-/-}$ mice (10, 11, 110). Interestingly, individuals affected by schizophrenia consistently show EEG abnormalities in γ and θ oscillations both under basal conditions and during sensory processing or execution of cognitive tasks (36, 111–114), as a possible result of a dysfunction of cortical GABAergic interneurons.

In summary, the present findings demonstrate that mGlu3 receptors are required for a proper development of GABAergic neurotransmission in the PFC and suggest that a dysfunction of these receptors alters the developmental trajectory of cortical GABAergic interneurons. They also suggest an association between such a dysfunction and long-lasting changes in thalamic and cortical networks underpinning quiet wakefulness and generation of EEG oscillations. It will be interesting to test the hypothesis that the genetic variants of GRM3 associated with psychiatric disorders alter the developmental trajectory of inhibitory neurotransmission in the PFC by causing changes in the expression or function of mGlu3 receptors. If so, an early treatment with drugs that selectively amplify mGlu3 receptor function in the appropriate temporal windows may be beneficial in individuals with hypomorphic GRM3 mutations.

This early treatment might represent a new strategy to correct the developmental abnormalities of GABAergic transmission associated with schizophrenia, taking into account that drugs that do not display cellular specificity in enhancing GABAergic transmission (*e.g.*, benzodiazepines or other $GABA_A$ receptor PAMs) are not effective in the treatment of psychotic disorders. A dysfunction of GABAergic interneurons of the PFC has been implicated in the pathophysiology of depression and stress-related disorders (115, 116), and mGlu2/3 receptor antagonists display antidepressant-like activity in animal models and are under clinical development for the treatment of major depression (117, 118). Thus, our findings may encourage the preclinical development of mGlu3 receptor negative allosteric modulators as potential antidepressant agents. FJ

ACKNOWLEDGMENTS

The authors thank Eli Lilly and Co. (Indianapolis, IN, USA) for kindly providing wild-type, $mGlu2^{-/-}$ and $mGlu3^{-/-}$ mice. This study was supported by funds from the Italian Ministry of Health (Ricerca Corrente 2019), the Alborada Trust (to T.W.), and Swedish Research Council (to T.W.). F.N. and M.C. are colast authors. S.M. and F.N. are coheads of the Associated International Laboratory (LIA): Perinatal Stress and Neurodegenerative Diseases, University of Lille, Centre National de la Recherche Scientifique (CNRS), Unité Mixte de Recherche (UMR) 8576, and Sapienza University of Rome/Istituto di Ricovero e Cura a Carattere Scientifico (IRCCS) Neuromed, France/Italy. The authors declare no conflicts of interest.

AUTHOR CONTRIBUTIONS

T. Imbriglio, R. Verhaeghe, K. Martinello, M. T. Pascarelli, G. Chece, D. Bucci, S. Notartomaso, M. Quattromani, G. Mascio, and F. Scalabrì performed research; A. Simeone, S. Maccari, and T. Wieloch contributed new reagents or analytic tools; C. Del Percio, S. Fucile, C. Babiloni, G. Battaglia, and C. Limatola analyzed data; C. Babiloni, F. Nicoletti, and M. Cannella wrote the paper; and F. Nicoletti and M. Cannella designed the research.

REFERENCES

1. Bruno, V., Caraci, F., Copani, A., Matrisciano, F., Nicoletti, F., and Battaglia, G. (2017) The impact of metabotropic glutamate receptors into active neurodegenerative processes: a "dark side" in the development of new symptomatic treatments for neurologic and psychiatric disorders. *Neuropharmacology* **115**, 180–192
2. Maksymetz, J., Moran, S. P., and Conn, P. J. (2017) Targeting metabotropic glutamate receptors for novel treatments of schizophrenia. *Mol. Brain* **10**, 15
3. Nicoletti, F., Bockaert, J., Collingridge, G. L., Conn, P. J., Ferraguti, F., Schoepp, D. D., Wroblewski, J. T., and Pin, J. P. (2011) Metabotropic glutamate receptors: from the workbench to the bedside. *Neuropharmacology* **60**, 1017–1041
4. Barnes, S. A., Pinto-Duarte, A., Kappe, A., Zembrzycki, A., Metzler, A., Mukamel, E. A., Lucero, J., Wang, X., Sejnowski, T. J., Markou, A., and Behrens, M. M. (2015) Disruption of mGluR5 in parvalbumin-positive interneurons induces core features of neurodevelopmental disorders. *Mol. Psychiatry* **20**, 1161–1172

5. Foster, D. J., and Conn, P. J. (2017) Allosteric modulation of GPCRs: new insights and potential utility for treatment of schizophrenia and other CNS disorders. *Neuron* **94**, 431–446
6. Bruno, V., Battaglia, G., Copani, A., D'Onofrio, M., Di Iorio, P., De Blasi, A., Melchiorri, D., Flor, P. J., and Nicoletti, F. (2001) Metabotropic glutamate receptor subtypes as targets for neuroprotective drugs. *J. Cereb. Blood Flow Metab.* **21**, 1013–1033
7. Kinon, B. J., Millen, B. A., Zhang, L., and McKinzie, D. L. (2015) Exploratory analysis for a targeted patient population responsive to the metabotropic glutamate 2/3 receptor agonist pomaglumetad methionil in schizophrenia. *Biol. Psychiatry* **78**, 754–762
8. Fell, M. J., Svensson, K. A., Johnson, B. G., and Schoepp, D. D. (2008) Evidence for the role of metabotropic glutamate (mGlu)2 not mGlu3 receptors in the preclinical antipsychotic pharmacology of the mGlu2/3 receptor agonist (-)-(1R,4S,5S,6S)-4-amino-2-sulfonylbicyclo[3.1.0]hexane-4,6-dicarboxylic acid (LY404039). *J. Pharmacol. Exp. Ther.* **326**, 209–217
9. Nikiforuk, A., Popik, P., Drescher, K. U., van Gaalen, M., Relo, A. L., Mezler, M., Marek, G., Schoemaker, H., Gross, G., and Bespalov, A. (2010) Effects of a positive allosteric modulator of group II metabotropic glutamate receptors, LY487379, on cognitive flexibility and impulsive-like responding in rats. *J. Pharmacol. Exp. Ther.* **335**, 665–673
10. Fujioka, R., Nii, T., Iwaki, A., Shibata, A., Ito, I., Kitaichi, K., Nomura, M., Hattori, S., Takao, K., Miyakawa, T., and Fukumaki, Y. (2014) Comprehensive behavioral study of mGluR3 knockout mice: implication in schizophrenia related endophenotypes. *Mol. Brain* **7**, 31
11. Lainiola, M., Procaccini, C., and Linden, A. M. (2014) mGluR3 knockout mice show a working memory defect and an enhanced response to MK-801 in the T- and Y-maze cognitive tests. *Behav. Brain Res.* **266**, 94–103
12. Corti, C., Crepaldi, L., Mion, S., Roth, A. L., Xuereb, J. H., and Ferraguti, F. (2007) Altered dimerization of metabotropic glutamate receptor 3 in schizophrenia. *Biol. Psychiatry* **62**, 747–755
13. Maj, C., Minelli, A., Giacopuzzi, E., Sacchetti, E., and Gennarelli, M. (2016) The role of metabotropic glutamate receptor genes in schizophrenia. *Curr. Neuropharmacol.* **14**, 540–550
14. Saini, S. M., Mancuso, S. G., Mostaid, M. S., Liu, C., Pantelis, C., Everall, I. P., and Bousman, C. A. (2017) Meta-analysis supports GWAS-implicated link between GRM3 and schizophrenia risk. *Transl. Psychiatry* **7**, e1196
15. Di Menna, L., Joffe, M. E., Iacovelli, L., Orlando, R., Lindsley, C. W., Mairesse, J., Gressèns, P., Cannella, M., Caraci, F., Copani, A., Bruno, V., Battaglia, G., Conn, P. J., and Nicoletti, F. (2018) Functional partnership between mGlu3 and mGlu5 metabotropic glutamate receptors in the central nervous system. *Neuropharmacology* **128**, 301–313
16. Ohishi, H., Shigemoto, R., Nakanishi, S., and Mizuno, N. (1993) Distribution of the mRNA for a metabotropic glutamate receptor (mGluR3) in the rat brain: an in situ hybridization study. *J. Comp. Neurol.* **335**, 252–266
17. Tanabe, Y., Nomura, A., Masu, M., Shigemoto, R., Mizuno, N., and Nakanishi, S. (1993) Signal transduction, pharmacological properties, and expression patterns of two rat metabotropic glutamate receptors, mGluR3 and mGluR4. *J. Neurosci.* **13**, 1372–1378
18. Tamaru, Y., Nomura, S., Mizuno, N., and Shigemoto, R. (2001) Distribution of metabotropic glutamate receptor mGluR3 in the mouse CNS: differential location relative to pre- and postsynaptic sites. *Neuroscience* **106**, 481–503
19. Catania, M. V., Landwehrmeyer, G. B., Testa, C. M., Standaert, D. G., Penney, J. B., Jr., and Young, A. B. (1994) Metabotropic glutamate receptors are differentially regulated during development. *Neuroscience* **61**, 481–495
20. Sohal, V. S., Zhang, F., Yizhar, O., and Deisseroth, K. (2009) Parvalbumin neurons and gamma rhythms enhance cortical circuit performance. *Nature* **459**, 698–702
21. Payne, J. A., Rivera, C., Voipio, J., and Kaila, K. (2003) Cation-chloride co-transporters in neuronal communication, development and trauma. *Trends Neurosci.* **26**, 199–206
22. Bandtlow, C. E., and Zimmermann, D. R. (2000) Proteoglycans in the developing brain: new conceptual insights for old proteins. *Physiol. Rev.* **80**, 1267–1290
23. Matthews, R. T., Kelly, G. M., Zerillo, C. A., Gray, G., Tiemeyer, M., and Hockfield, S. (2002) Aggrecan glycoforms contribute to the molecular heterogeneity of perineuronal nets. *J. Neurosci.* **22**, 7536–7547
24. McRae, P. A., Rocco, M. M., Kelly, G., Brumberg, J. C., and Matthews, R. T. (2007) Sensory deprivation alters aggrecan and perineuronal net expression in the mouse barrel cortex. *J. Neurosci.* **27**, 5405–5413
25. Brückner, G., Grosche, J., Schmidt, S., Härtig, W., Margolis, R. U., Delpech, B., Seidenbecher, C. I., Czaniera, R., and Schachner, M. (2000) Postnatal development of perineuronal nets in wild-type mice and in a mutant deficient in tenascin-R. *J. Comp. Neurol.* **428**, 616–629
26. Pizzorusso, T., Medini, P., Berardi, N., Chierzi, S., Fawcett, J. W., and Maffei, L. (2002) Reactivation of ocular dominance plasticity in the adult visual cortex. *Science* **298**, 1248–1251
27. Slaker, M., Churchill, L., Todd, R. P., Blacktop, J. M., Zuloaga, D. G., Raber, J., Darling, R. A., Brown, T. E., and Sorg, B. A. (2015) Removal of perineuronal nets in the medial prefrontal cortex impairs the acquisition and reconsolidation of a cocaine-induced conditioned place preference memory. *J. Neurosci.* **35**, 4190–4202
28. Paylor, J. W., Wendlandt, E., Freeman, T. S., Greba, Q., Marks, W. N., Howland, J. G., and Winship, I. R. (2018) Impaired cognitive function after perineuronal net degradation in the medial prefrontal cortex. *eNeuro* **5**, ENEURO.0253-18.2018
29. Jiang, Z., Cowell, R. M., and Nakazawa, K. (2013) Convergence of genetic and environmental factors on parvalbumin-positive interneurons in schizophrenia. *Front. Behav. Neurosci.* **7**, 116
30. Hashimoto, T., Volk, D. W., Eggan, S. M., Mirnics, K., Pierri, J. N., Sun, Z., Sampson, A. R., and Lewis, D. A. (2003) Gene expression deficits in a subclass of GABA neurons in the prefrontal cortex of subjects with schizophrenia. *J. Neurosci.* **23**, 6315–6326
31. Hashimoto, T., Arion, D., Unger, T., Maldonado-Avilés, J. G., Morris, H. M., Volk, D. W., Mirnics, K., and Lewis, D. A. (2008) Alterations in GABA-related transcriptome in the dorsolateral prefrontal cortex of subjects with schizophrenia. *Mol. Psychiatry* **13**, 147–161
32. Pérez-Santiago, J., Diez-Alarcia, R., Callado, L. F., Zhang, J. X., Chana, G., White, C. H., Glatt, S. J., Tsuang, M. T., Everall, I. P., Meana, J. J., and Woelk, C. H. (2012) A combined analysis of microarray gene expression studies of the human prefrontal cortex identifies genes implicated in schizophrenia. *J. Psychiatr. Res.* **46**, 1464–1474
33. Glausier, J. R., Fish, K. N., and Lewis, D. A. (2014) Altered parvalbumin basket cell inputs in the dorsolateral prefrontal cortex of schizophrenia subjects. *Mol. Psychiatry* **19**, 30–36; erratum: 140
34. Enwright J. F. III, Sanapala, S., Foglio, A., Berry, R., Fish, K. N., and Lewis, D. A. (2016) Reduced labeling of parvalbumin neurons and perineuronal nets in the dorsolateral prefrontal cortex of subjects with schizophrenia. *Neuropsychopharmacology* **41**, 2206–2214
35. Arnsten, A. F., and Jin, L. E. (2014) Molecular influences on working memory circuits in dorsolateral prefrontal cortex. *Prog. Mol. Biol. Transl. Sci.* **122**, 211–231
36. Uhlhaas, P. J., and Singer, W. (2010) Abnormal neural oscillations and synchrony in schizophrenia. *Nat. Rev. Neurosci.* **11**, 100–113
37. Curley, A. A., and Lewis, D. A. (2012) Cortical basket cell dysfunction in schizophrenia. *J. Physiol.* **590**, 715–724
38. Pantazopoulos, H., Woo, T. U., Lim, M. P., Lange, N., and Berretta, S. (2010) Extracellular matrix-glial abnormalities in the amygdala and entorhinal cortex of subjects diagnosed with schizophrenia. *Arch. Gen. Psychiatry* **67**, 155–166
39. Berretta, S. (2012) Extracellular matrix abnormalities in schizophrenia. *Neuropharmacology* **62**, 1584–1597
40. Berretta, S., Pantazopoulos, H., Markota, M., Brown, C., and Batzianouli, E. T. (2015) Losing the sugar coating: potential impact of perineuronal net abnormalities on interneurons in schizophrenia. *Schizophr. Res.* **167**, 18–27
41. Mauney, S. A., Athanas, K. M., Pantazopoulos, H., Shaskan, N., Passeri, E., Berretta, S., and Woo, T. U. (2013) Developmental pattern of perineuronal nets in the human prefrontal cortex and their deficit in schizophrenia. *Biol. Psychiatry* **74**, 427–435
42. Linden, A. M., Shannon, H., Baez, M., Yu, J. L., Koester, A., and Schoepp, D. D. (2005) Anxiolytic-like activity of the mGLU2/3 receptor agonist LY354740 in the elevated plus maze test is disrupted in metabotropic glutamate receptor 2 and 3 knock-out mice. *Psychopharmacology (Berl.)* **179**, 284–291
43. Paxinos, G., and Watson, C. (2007) *The Rat Brain in Stereotaxic Coordinates*, 6th ed., Academic Press, London
44. Bucci, D., Busceti, C. L., Calierno, M. T., Di Pietro, P., Madonna, M., Biagioni, F., Ryskalin, L., Limanaqi, F., Nicoletti, F., and Fornai, F.

(2017) Systematic morphometry of catecholamine nuclei in the brainstem. *Front. Neuroanat.* **11**, 98
45. Gundersen, H. J., and Jensen, E. B. (1987) The efficiency of systematic sampling in stereology and its prediction. *J. Microsc.* **147**, 229–263
46. Quattromani, M. J., Pruvost, M., Guerreiro, C., Backlund, F., Englund, E., Aspberg, A., Jaworski, T., Hakon, J., Ruscher, K., Kaczmarek, L., Vivien, D., and Wieloch, T. (2018) Extracellular matrix modulation is driven by experience-dependent plasticity during stroke recovery. *Mol. Neurobiol.* **55**, 2196–2213
47. Khirug, S., Yamada, J., Afzalov, R., Voipio, J., Khiroug, L., and Kaila, K. (2008) GABAergic depolarization of the axon initial segment in cortical principal neurons is caused by the Na-K-2Cl cotransporter NKCC1. *J. Neurosci.* **28**, 4635–4639
48. Del Percio, C., Drinkenburg, W., Lopez, S., Infarinato, F., Bastlund, J. F., Laursen, B., Pedersen, J. T., Christensen, D. Z., Forloni, G., Frasca, A., Noè, F. M., Bentivoglio, M., Fabene, P. F., Bertini, G., Colavito, V., Kelley, J., Dix, S., Richardson, J. C., and Babiloni, C.; PharmaCog Consortium. (2017) On-going electroencephalographic rhythms related to cortical arousal in wild-type mice: the effect of aging. *Neurobiol. Aging* **49**, 20–30
49. Del Percio, C., Drinkenburg, W., Lopez, S., Limatola, C., Bastlund, J. F., Christensen, D. Z., Pedersen, J. T., Forloni, G., Frasca, A., Noe, F. M., Bentivoglio, M., Fabene, P. F., Bertini, G., Colavito, V., Dix, S., Ferri, R., Bordet, R., Richardson, J. C., and Babiloni, C. (2018) Ongoing electroencephalographic activity associated with cortical arousal in transgenic PDAPP mice (hAPP V717F). *Curr. Alzheimer Res.* **15**, 259–272
50. Guillemot, F., and Joyner, A. L. (1993) Dynamic expression of the murine Achaete-Scute homologue Mash-1 in the developing nervous system. *Mech. Dev.* **42**, 171–185
51. Cau, E., Gradwohl, G., Fode, C., and Guillemot, F. (1997) Mash1 activates a cascade of bHLH regulators in olfactory neuron progenitors. *Development* **124**, 1611–1621
52. Hirsch, M. R., Tiveron, M. C., Guillemot, F., Brunet, J. F., and Goridis, C. (1998) Control of noradrenergic differentiation and Phox2a expression by MASH1 in the central and peripheral nervous system. *Development* **125**, 599–608
53. Golding, B., Pouchelon, G., Bellone, C., Murthy, S., Di Nardo, A. A., Govindan, S., Ogawa, M., Shimogori, T., Lüscher, C., Dayer, A., and Jabaudon, D. (2014) Retinal input directs the recruitment of inhibitory interneurons into thalamic visual circuits. *Neuron* **81**, 1057–1069; erratum: 1443
54. Hensch, T. K., Fagiolini, M., Mataga, N., Stryker, M. P., Baekkeskov, S., and Kash, S. F. (1998) Local GABA circuit control of experience-dependent plasticity in developing visual cortex. *Science* **282**, 1504–1508
55. Bernard, C., and Prochiantz, A. (2016) Otx2-PNN interaction to regulate cortical plasticity. *Neural Plast.* **2016**, 7931693
56. Bernard, C., Vincent, C., Testa, D., Bertini, E., Ribot, J., Di Nardo, A. A., Volovitch, M., and Prochiantz, A. (2016a) A mouse model for conditional secretion of specific single-chain antibodies provides genetic evidence for regulation of cortical plasticity by a non-cell autonomous homeoprotein transcription factor. *PLoS Genet.* **12**, e1006035
57. Sakai, A., Nakato, R., Ling, Y., Hou, X., Hara, N., Iijima, T., Yanagawa, Y., Kuwano, R., Okuda, S., Shirahige, K., and Sugiyama, S. (2017) Genome-wide target analyses of Otx2 homeoprotein in postnatal cortex. *Front. Neurosci.* **11**, 307
58. Kroll, T. T., and O'Leary, D. D. (2005) Ventralized dorsal telencephalic progenitors in Pax6 mutant mice generate GABA interneurons of a lateral ganglionic eminence fate. *Proc. Natl. Acad. Sci. USA* **102**, 7374–7379
59. Gopal, P. P., and Golden, J. A. (2008) $Pax6^{-/-}$ mice have a cell nonautonomous defect in nonradial interneuron migration. *Cereb. Cortex* **18**, 752–762
60. Sussel, L., Marin, O., Kimura, S., and Rubenstein, J. L. (1999) Loss of Nkx2.1 homeobox gene function results in a ventral to dorsal molecular respecification within the basal telencephalon: evidence for a transformation of the pallidum into the striatum. *Development* **126**, 3359–3370
61. Xu, Q., Cobos, I., De La Cruz, E., Rubenstein, J. L., and Anderson, S. A. (2004) Origins of cortical interneuron subtypes. *J. Neurosci.* **24**, 2612–2622
62. Butt, S. J., Sousa, V. H., Fuccillo, M. V., Hjerling-Leffler, J., Miyoshi, G., Kimura, S., and Fishell, G. (2008) The requirement of Nkx2-1 in the temporal specification of cortical interneuron subtypes. *Neuron* **59**, 722–732
63. Du, T., Xu, Q., Ocbina, P. J., and Anderson, S. A. (2008) NKX2.1 specifies cortical interneuron fate by activating Lhx6. *Development* **135**, 1559–1567
64. Hilbig, H., Bidmon, H. J., Blohm, U., and Zilles, K. (2001) Wisteria floribunda agglutinin labeling patterns in the human cortex: a tool for revealing areal borders and subdivisions in parallel with immunocytochemistry. *Anat. Embryol. (Berl.)* **203**, 45–52
65. Khirug, S., Huttu, K., Ludwig, A., Smirnov, S., Voipio, J., Rivera, C., Kaila, K., and Khiroug, L. (2005) Distinct properties of functional KCC2 expression in immature mouse hippocampal neurons in culture and in acute slices. *Eur. J. Neurosci.* **21**, 899–904
66. Rivera, C., Voipio, J., Payne, J. A., Ruusuvuori, E., Lahtinen, H., Lamsa, K., Pirvola, U., Saarma, M., and Kaila, K. (1999) The K^+/Cl^- co-transporter KCC2 renders GABA hyperpolarizing during neuronal maturation. *Nature* **397**, 251–255
67. Stein, V., Hermans-Borgmeyer, I., Jentsch, T. J., and Hübner, C. A. (2004) Expression of the KCl cotransporter KCC2 parallels neuronal maturation and the emergence of low intracellular chloride. *J. Comp. Neurol.* **468**, 57–64
68. Uvarov, P., Pruunsild, P., Timmusk, T., and Airaksinen, M. S. (2005) Neuronal K^+/Cl^- co-transporter (KCC2) transgenes lacking neurone restrictive silencer element recapitulate CNS neurone-specific expression and developmental up-regulation of endogenous KCC2 gene. *J. Neurochem.* **95**, 1144–1155
69. Wong, F. K., Bercsenyi, K., Sreenivasan, V., Portalés, A., Fernández-Otero, M., and Marín, O. (2018) Pyramidal cell regulation of interneuron survival sculpts cortical networks. *Nature* **557**, 668–673
70. Ueno, H., Suemitsu, S., Okamoto, M., Matsumoto, Y., and Ishihara, T. (2017) Parvalbumin neurons and perineuronal nets in the mouse prefrontal cortex. *Neuroscience* **343**, 115–127
71. Miyamae, T., Chen, K., Lewis, D. A., and Gonzalez-Burgos, G. (2017) Distinct physiological maturation of parvalbumin-positive neuron subtypes in mouse prefrontal cortex. *J. Neurosci.* **37**, 4883–4902
72. Moghaddam, B., and Javitt, D. (2012) From revolution to evolution: the glutamate hypothesis of schizophrenia and its implication for treatment. *Neuropsychopharmacology* **37**, 4–15
73. Pi, H. J., Hangya, B., Kvitsiani, D., Sanders, J. I., Huang, Z. J., and Kepecs, A. (2013) Cortical interneurons that specialize in disinhibitory control. *Nature* **503**, 521–524
74. Wang, Y., Toledo-Rodriguez, M., Gupta, A., Wu, C., Silberberg, G., Luo, J., and Markram, H. (2004) Anatomical, physiological and molecular properties of Martinotti cells in the somatosensory cortex of the juvenile rat. *J. Physiol.* **561**, 65–90
75. Chiu, C. Q., Lur, G., Morse, T. M., Carnevale, N. T., Ellis-Davies, G. C., and Higley, M. J. (2013) Compartmentalization of GABAergic inhibition by dendritic spines. *Science* **340**, 759–762
76. Földy, C., Lee, S. Y., Szabadics, J., Neu, A., and Soltesz, I. (2007) Cell type-specific gating of perisomatic inhibition by cholecystokinin. *Nat. Neurosci.* **10**, 1128–1130
77. Marsh, E. D., Nasrallah, M. P., Walsh, C., Murray, K. A., Nicole Sunnen, C., McCoy, A., and Golden, J. A. (2016) Developmental interneuron subtype deficits after targeted loss of Arx. *BMC Neurosci.* **17**, 35
78. Kon, E., Cossard, A., and Jossin, Y. (2017) Neuronal polarity in the embryonic mammalian cerebral cortex. *Front. Cell. Neurosci.* **11**, 163
79. Ishii, K., Kubo, K. I., and Nakajima, K. (2016) Reelin and neuropsychiatric disorders. *Front. Cell. Neurosci.* **10**, 229
80. Grayson, D. R., Jia, X., Chen, Y., Sharma, R. P., Mitchell, C. P., Guidotti, A., and Costa, E. (2005) Reelin promoter hypermethylation in schizophrenia. *Proc. Natl. Acad. Sci. USA* **102**, 9341–9346
81. Woo, T. U., Miller, J. L., and Lewis, D. A. (1997) Schizophrenia and the parvalbumin-containing class of cortical local circuit neurons. *Am. J. Psychiatry* **154**, 1013–1015
82. Lewis, D. A., Hashimoto, T., and Morris, H. M. (2008) Cell and receptor type-specific alterations in markers of GABA neurotransmission in the prefrontal cortex of subjects with schizophrenia. *Neurotox. Res.* **14**, 237–248
83. Gonzalez-Burgos, G., Cho, R. Y., and Lewis, D. A. (2015) Alterations in cortical network oscillations and parvalbumin neurons in schizophrenia. *Biol. Psychiatry* **77**, 1031–1040
84. Volk, D. W., Edelson, J. R., and Lewis, D. A. (2016) Altered expression of developmental regulators of parvalbumin and

somatostatin neurons in the prefrontal cortex in schizophrenia. *Schizophr. Res.* **177**, 3–9
85. Belforte, J. E., Zsiros, V., Sklar, E. R., Jiang, Z., Yu, G., Li, Y., Quinlan, E. M., and Nakazawa, K. (2010) Postnatal NMDA receptor ablation in corticolimbic interneurons confers schizophrenia-like phenotypes. *Nat. Neurosci.* **13**, 76–83
86. Sullivan, C. R., Funk, A. J., Shan, D., Haroutunian, V., and McCullumsmith, R. E. (2015) Decreased chloride channel expression in the dorsolateral prefrontal cortex in schizophrenia. *PLoS One* **10**, e0123158
87. Merner, N. D., Chandler, M. R., Bourassa, C., Liang, B., Khanna, A. R., Dion, P., Rouleau, G. A., and Kahle, K. T. (2015) Regulatory domain or CpG site variation in SLC12A5, encoding the chloride transporter KCC2, in human autism and schizophrenia. *Front. Cell. Neurosci.* **9**, 386
88. Amin, H., Marinaro, F., De Pietri Tonelli, D., and Berdondini, L. (2017) Developmental excitatory-to-inhibitory GABA-polarity switch is disrupted in 22q11.2 deletion syndrome: a potential target for clinical therapeutics. *Sci. Rep.* **7**, 15752
89. Yabuno, K., Morise, J., Kizuka, Y., Hashii, N., Kawasaki, N., Takahashi, S., Miyata, S., Izumikawa, T., Kitagawa, H., Takematsu, H., and Oka, S. (2015) A sulfated glycosaminoglycan linkage region is a novel type of human natural killer-1 (HNK-1) epitope expressed on aggrecan in perineuronal nets. *PLoS One* **10**, e0144560
90. Yamada, J., Ohgomori, T., and Jinno, S. (2017) Alterations in expression of Cat-315 epitope of perineuronal nets during normal ageing, and its modulation by an open-channel NMDA receptor blocker, memantine. *J. Comp. Neurol.* **525**, 2035–2049
91. Härtig, W., Brauer, K., and Brückner, G. (1992) Wisteria floribunda agglutinin-labelled nets surround parvalbumin-containing neurons. *Neuroreport* **3**, 869–872
92. Haji-Ghassemi, O., Gilbert, M., Spence, J., Schur, M. J., Parker, M. J., Jenkins, M. L., Burke, J. E., van Faassen, H., Young, N. M., and Evans, S. V. (2016) Molecular basis for recognition of the cancer glycobiomarker, LacdiNAc (GalNAc[β1→4]GlcNAc), by Wisteria floribunda Agglutinin. *J. Biol. Chem.* **291**, 24085–24095
93. Miyata, S., Nadanaka, S., Igarashi, M., and Kitagawa, H. (2018) Structural variation of chondroitin sulfate chains contributes to the molecular heterogeneity of perineuronal nets. *Front. Integr. Nuerosci.* **12**, 3
94. Happel, M. F., and Frischknecht, R. (2016) Neuronal plasticity in the juvenile and adult brain regulated by the extracellular matrix. In *Composition and Function of the Extracellular Matrix in the Human Body* (Travascio, F., ed.), pp. 143–158, INTECH, Rijeka, Croatia
95. Bozzelli, P. L., Alaiyed, S., Kim, E., Villapol, S., and Conant, K. (2018) Proteolytic remodeling of perineuronal nets: effects on synaptic plasticity and neuronal population dynamics. *Neural Plast.* **2018**, 5735789
96. Jin, L. E., Wang, M., Yang, S. T., Yang, Y., Galvin, V. C., Lightbourne, T. C., Ottenheimer, D., Zhong, Q., Stein, J., Raja, A., Paspalas, C. D., and Arnsten, A. F. T. (2017) mGluR2/3 mechanisms in primate dorsolateral prefrontal cortex: evidence for both presynaptic and postsynaptic actions. *Mol. Psychiatry* **22**, 1615–1625
97. Walker, A. G., and Conn, P. J. (2015) Group I and group II metabotropic glutamate receptor allosteric modulators as novel potential antipsychotics. *Curr. Opin. Pharmacol.* **20**, 40–45
98. Egan, M. F., Straub, R. E., Goldberg, T. E., Yakub, I., Callicott, J. H., Hariri, A. R., Mattay, V. S., Bertolino, A., Hyde, T. M., Shannon-Weickert, C., Akil, M., Crook, J., Vakkalanka, R. K., Balkissoon, R., Gibbs, R. A., Kleinman, J. E., and Weinberger, D. R. (2004) Variation in GRM3 affects cognition, prefrontal glutamate, and risk for schizophrenia. *Proc. Natl. Acad. Sci. USA* **101**, 12604–12609
99. Harrison, P. J., Lyon, L., Sartorius, L. J., Burnet, P. W., and Lane, T. A. (2008) The group II metabotropic glutamate receptor 3 (mGluR3, mGlu3, GRM3): expression, function and involvement in schizophrenia. *J. Psychopharmacol. (Oxford)* **22**, 308–322
100. Battaglia, G., Molinaro, G., Riozzi, B., Storto, M., Busceti, C. L., Spinsanti, P., Bucci, D., Di Liberto, V., Mudò, G., Corti, C., Corsi, M., Nicoletti, F., Belluardo, N., and Bruno, V. (2009) Activation of mGlu3 receptors stimulates the production of GDNF in striatal neurons. *PLoS One* **4**, e6591
101. Battaglia, G., Riozzi, B., Bucci, D., Di Menna, L., Molinaro, G., Pallottino, S., Nicoletti, F., and Bruno, V. (2015) Activation of mGlu3 metabotropic glutamate receptors enhances GDNF and GLT-1 formation in the spinal cord and rescues motor neurons in the SOD-1 mouse model of amyotrophic lateral sclerosis. *Neurobiol. Dis.* **74**, 126–136
102. Canty, A. J., Dietze, J., Harvey, M., Enomoto, H., Milbrandt, J., and Ibáñez, C. F. (2009) Regionalized loss of parvalbumin interneurons in the cerebral cortex of mice with deficits in GFRalpha1 signaling. *J. Neurosci.* **29**, 10695–10705
103. Perrinjaquet, M., Sjöstrand, D., Moliner, A., Zechel, S., Lamballe, F., Maina, F., and Ibáñez, C. F. (2011) MET signaling in GABAergic neuronal precursors of the medial ganglionic eminence restricts GDNF activity in cells that express GFRα1 and a new transmembrane receptor partner. *J. Cell Sci.* **124**, 2797–2805
104. Kandel, A., and Buzsáki, G. (1997) Cellular-synaptic generation of sleep spindles, spike-and-wave discharges, and evoked thalamocortical responses in the neocortex of the rat. *J. Neurosci.* **17**, 6783–6797
105. Hughes, S. W., and Crunelli, V. (2005) Thalamic mechanisms of EEG alpha rhythms and their pathological implications. *Neuroscientist* **11**, 357–372
106. Lorincz, M. L., Kékesi, K. A., Juhász, G., Crunelli, V., and Hughes, S. W. (2009) Temporal framing of thalamic relay-mode firing by phasic inhibition during the alpha rhythm. *Neuron* **63**, 683–696
107. Crunelli, V., David, F., Lőrincz, M. L., and Hughes, S. W. (2015) The thalamocortical network as a single slow wave-generating unit. *Curr. Opin. Neurobiol.* **31**, 72–80
108. Nyíri, G., Freund, T. F., and Somogyi, P. (2001) Input-dependent synaptic targeting of alpha(2)-subunit-containing GABA(A) receptors in synapses of hippocampal pyramidal cells of the rat. *Eur. J. Neurosci.* **13**, 428–442
109. Del Pino, I., Brotons-Mas, J. R., Marques-Smith, A., Marighetto, A., Frick, A., Marín, O., and Rico, B. (2017) Abnormal wiring of CCK^+ basket cells disrupts spatial information coding. *Nat. Neurosci.* **20**, 784–792
110. Pritchett, D., Jagannath, A., Brown, L. A., Tam, S. K., Hasan, S., Gatti, S., Harrison, P. J., Bannerman, D. M., Foster, R. G., and Peirson, S. N. (2015) Deletion of metabotropic glutamate receptors 2 and 3 (mGlu2 & mGlu3) in mice disrupts sleep and wheel-running activity, and increases the sensitivity of the circadian system to light. *PLoS One* **10**, e0125523
111. Schmiedt, C., Brand, A., Hildebrandt, H., and Basar-Eroglu, C. (2005) Event-related theta oscillations during working memory tasks in patients with schizophrenia and healthy controls. *Brain Res. Cogn. Brain Res.* **25**, 936–947
112. Cho, R. Y., Konecky, R. O., and Carter, C. S. (2006) Impairments in frontal cortical gamma synchrony and cognitive control in schizophrenia. *Proc. Natl. Acad. Sci. USA* **103**, 19878–19883
113. Haenschel, C., Bittner, R. A., Waltz, J., Haertling, F., Wibral, M., Singer, W., Linden, D. E., and Rodriguez, E. (2009) Cortical oscillatory activity is critical for working memory as revealed by deficits in early-onset schizophrenia. *J. Neurosci.* **29**, 9481–9489
114. Minzenberg, M. J., Firl, A. J., Yoon, J. H., Gomes, G. C., Reinking, C., and Carter, C. S. (2010) Gamma oscillatory power is impaired during cognitive control independent of medication status in first-episode schizophrenia. *Neuropsychopharmacology* **35**, 2590–2599
115. Duman, R. S., Sanacora, G., and Krystal, J. H. (2019) Altered connectivity in depression: GABA and glutamate neurotransmitter deficits and reversal by novel treatments. *Neuron* **102**, 75–90
116. Fogaça, M. V., and Duman, R. S. (2019) Cortical GABAergic dysfunction in stress and depression: new insights for therapeutic interventions. *Front. Cell. Neurosci.* **13**, 87
117. Chaki, S., and Fukumoto, K. (2018) mGlu receptors as potential targets for novel antidepressants. *Curr. Opin. Pharmacol.* **38**, 24–30
118. Chaki, S. (2017) mGlu2/3 Receptor antagonists as novel antidepressants. *Trends Pharmacol. Sci.* **38**, 569–580

Received for publication April 29, 2019.
Accepted for publication September 17, 2019.